EllipseFit 3
User Manual

Table of Contents

License and Citation

License
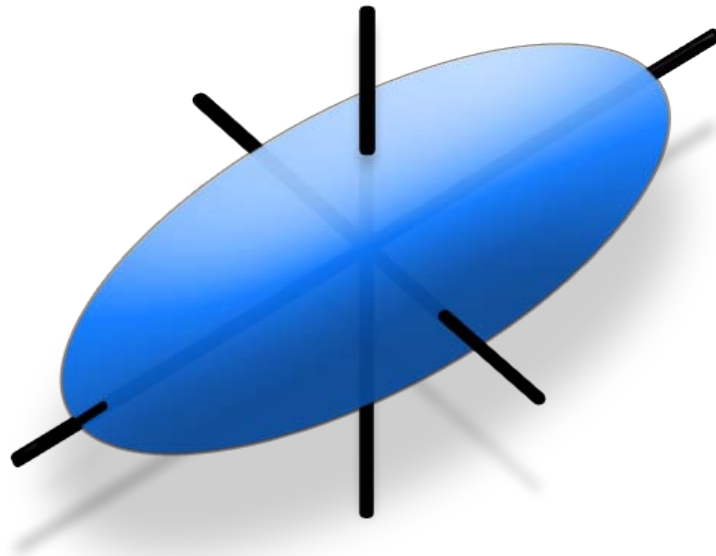
EllipseFit 3 software and accompanying documentation are Copyright © Frederick W. Vollmer. They come with no warrantees or guarantees of any kind. The software is free and may be downloaded and used without cost, however the author retains all rights to the source, binary code and accompanying files. It may not be redistributed or posted online. It is requested that acknowledgment and citation be given for any usage that leads to publication.

This software and any related documentation are provided "as is" without warranty of any kind, either express or implied, including, without limitation, the implied warranties or merchantability, fitness for a particular purpose, or non-infringement. The entire risk arising out of use or performance of the software remains with you.

Citation

EllipseFit is the result of many hours of work over several decades. Algorithms used in the program come from numerous sources, however many have been developed by the author, some of which have not yet been published and are the subject of papers in preparations. I have released the program publicly with the hope that the structure and tectonics community will find it useful, and ask forgiveness for the limited documentation, as well as respect for publication priority.

In return for free use, I request that any significant use of the software in analyzing data or preparing diagrams be cited and acknowledged in publications, presentations, or other works. An acknowledgement could be, "I thank Frederick W. Vollmer for the use of his EllipseFit 3 software."

Appropriate references include (see References):

Vollmer (2010) discusses ellipse and ellipse fitting techniques, including Shan's method, and their implementation in EllipseFit.
Vollmer (2011a) discusses methods for contouring finite strain on the unit hyperboloid and the use of hyperboloidal stereographic, equal-area and other projections for strain analysis.
Vollmer (2011b) discusses best-fit strain from multiple angles of shear and an analytical solution to the Wellman diagram.

A suitable references to the software and this documentation, are:

Vollmer, F.W., 2014. EllipseFit 3.1.0. http://www.frederickvollmer.com/ellipsefit/.
Vollmer, F.W., 2014. EllipseFit 3.1.0 User Manual. http://www.frederickvollmer.com/ellipsefit/.

Registration

Please consider registering the software, registration is free and helps me determine the software usage and justify the time spent in it's upkeep. To register, simply send an email to me at vollmerf@gmail.com with your user name, affiliation, and usage. I will send you one email in reply with my thanks, and will not place you on a mailing list. For example, send me an email with something like:

User: Frederick Vollmer
Affiliation: SUNY New Paltz, Geology Department
Usage: Undergraduate structural geology course and research

I am happy to take emails with questions and suggestions, either at the university (SUNY New Paltz) or at the gmail address used on my website. However I am not reliable about checking email, so please forgive me if I am slow in answering, I will try to respond in as timely a fashion as possible.

1. Introduction

EllipseFit is an integrated program for geological finite strain analysis. It is used for determining two and three-dimensional strain from oriented photographs, and is designed for field and laboratory based structural geology studies. The graphical interface and multi-platform deployment also make it ideal for introductory or advanced structural geology laboratories. I use the software to teach structural geology at SUNY New Paltz, where hundreds of students have used it in laboratory and field studies. EllipseFit is currently implemented for Windows 32, Macintosh 10.5+, and Linux (Ubuntu) 64 bit platforms.

EllipseFit is suitable for determining two and three dimensional strain using various objects including center points (Fry analysis), lines, ellipses, and polygons. Polygons include ooids, pebbles, fossils, or particles of *any* initial shape. The analysis of strain from polygons is widely applicable to many rocks in thin section, hand sample, or suitable outcrops. EllipseFit allows digitizing polygons directly, or indirectly by using a flood fill method. EllipseFit converts them to moment equivalent ellipses, and the mean ellipse is equivalent to the strain (Mulchrone and Choudhury, 2004). Given three or more oriented sections EllipseFit can calculate the three dimensional strain using the method of Shan (2008).

This User Manual was prepared for the strain workshop at the *2014 Structural Geology and Tectonics Forum*, at the Colorado School of Mines with Paul Karabinos and Matty Mookerjee, and is not , however, complete. EllipseFit 3 has numerous improvements over version 2, but has had more limited testing. Additional releases are planned in the near future. Version 2 is stable and has been widely used, including for a strain workshop at the *2012 Structural Geology and Tectonics Forum* at Williams College. No updates are planned for EllipseFit 2.

I am a professor of structural geology, and have taught for over 30 years at SUNY New Paltz. I had the luck to be introduced to analytical structural geology as a student, and am particularly grateful to my mentors Rob Twiss at UC Davis, Win Means at SUNY Albany, and Peter Hudleston at U Minnesota whose clear thinking inspired me. I was introduced to programming as a grade school student, when my dear mother forced me to take a summer school course. I subsequently joined the Computer Club, as the third member, and spent countless hours on the terminal connected remotely to a mainframe. Writing code is still an obsession.

Version 1 of EllipseFit was written in the early 1980s in C++ for Macintosh, in part based on code from a Fortran program written (on punch cards) for Win Means. Version 2 was written in cross platform RealBasic, however issues with licensing, cost, performance, and the closed source led me to abandon that language. Version 3 is fully rewritten, with tens of thousands of lines of code, in Free Pascal, a professional open source compiler that runs on over 40 operating systems. This allows improved code with better speed and extensibility, and the potential to port to other platforms. I simultaneously develop several programs that use common graphics and matrix libraries that I have written.

1.1 Installation

On Macintosh OS X, double click the disk image file (.dmg), and drag the EllipseFit application to your Applications folder, or other desired location.

On Windows, unzip the zip file (.zip) using the *Extract All* option, and drag the EllipseFit folder to any desired location. The EllipseFit folder contains the EllipseFit application (EllipseFit.exe), and a "Resources" folder which is required. Please make sure to entirely extract the EllipseFit folder from the zip file, this is the most common installation problem.

On Linux unpack the gzip file (.tar.gz), and copy the EllipseFit folder to any desired location. The EllipseFit folder contains the EllipseFit application (ellipsefit), and a "Resources" folder which is required. An application icon (ellipsefit.png) is included in the Resources folder if desired for installation.

There is also a folder of example data and images to show how data is formatted, these are referred to in this guide. After installing a new version it is recommended that you reset the preferences using the "Reset Preferences" command in the Help menu. This will clear any options that may have changed and set them to default values. The preferences are stored in the file EllipseFit3.xml, which is located in the folder EllipseFit in your operating system's application preferences folder. To deinstall simply delete the EllipseFit application folder, and optionally delete the preference folder. No other files are installed on your computer. No administrative permissions are required to install EllipseFit, and it is possible to keep a copy on a thumb drive to run on any computer.

1.2   Example Data Files

The included example files and images can be used to determine input data formats. These are simple files that can be generated using a text editor or spreadsheet. EllipseFit 3 will read comma separated (csv), tab separated (tsv), and Open Document (ods) formats. The header line indicates the type of data required in each column. The included example files are named to indicate their contents (this is not required, EllipseFit will examine the headers to determine the available data, and extra columns are ignored):

E2 - Ramsay and Huber 1983 (small).csv
E2 - Ramsay and Huber 1983 (small).jpg
E2 - Ramsay and Huber 1983 (large).jpg
Example ellipse data and thin section photomicrograph (from Ramsay and Huber, 1983). This data type can contain (X, Y) coordinates for Fry-type analyses, or complete ellipse data including (X, Y, A, B, R, Phi) axes data. Note that there are small and large versions, I use the large version, which does not include a data file, for teaching.

E3 - Hossack 1968.csv
Example ellipsoid data (from Hossack, 1968) with (A, B, C) axes data for Flinn and Nadai graphs.

ES - Owens 1984.csv
Example ellipse section data (fron Owens, 1984) for calculating the three-dimensional strain ellipsoid from three or more faces using Shan's (2008) method. The strikes and dips of each section must be included.

LA - Ragan 1985 F10.1a.csv
LA - Ragan 1985 F10.1a.png
Example line angular shear data and image (from Ragan, 1985) for analytical Wellman-type analysis (Vollmer, 2011). Each data point requires the endpoints of two lines that originally had a constant angle. This is an analytical solution to the classic multiple brachiopod problem illustrated in a number of structural geology texts.

LS - Ragan 2009 T14.9.csv
Example line stretch data for lines with known initial and final lengths, such as boudins and folds. EllipseFit does not yet provide digitizing of this type of data. Please contact me if this would be of interest. Note that the LS data is from fold flattening index example (Ragan, 2009), which is

mathematically related.

MLLF Test 60.csv
Sample of 60 points used to test the maximum mean log likelihood function (MLLF) method of Shan and Xiao (2011).

2.   Overview of Strain Analysis

Geological strain analysis and theory is an important aspect of structural geology that is covered in numerous textbooks (e.g., Means, 1976; Hobbs, Means, and Williams, 1976; Ragan, 1985; Marshak and Mitra, 1988; Van der Pluijm and Marshak, 2004; Pollard and Fletcher, 2005; Twiss and Moores, 2007; Ragan, 2009; Fossen, 2010). Ragan (2009) and Ramsay and Huber (1983) provide excellent overviews of techniques for the analysis of strain in deformed rocks. The literature is vast, but in the references I have tried to included many of the papers that are relevant to using EllipseFit.

The following chapters discuss techniques of strain analysis that are implemented in EllipseFit in terms of the type of data collected: *points, lines, ellipses*, and *polygons*. Points are the simplest type of data collected, however, as discussed in Chapter 3, *Strain from Points*, it can be difficult to objectively extract strain from point distributions. A new objective procedure, *mean log likelihood function*, or MLLF, maximization (Shan and Xiao, 2011) has been added in version 3.1. The analysis of line data depends on the known initial lengths of, or angles between, lines, and has important applications for some data as discussed in Chapter 4, *Strain from Lines*.

Chapter 5, *Strain from Ellipses and Polygons*, covers ellipse data, which is collected assuming that particles, such as sand grains, initially approximated a collection of random spheres or ellipsoids. It turns out, however, that ellipse data is a subcategory of polygon data. An important mathematical proof (Mulchrone and Choudhury, 2004) shows that all particles, *of any shape*, that can be assumed to have been initially randomly oriented, can be used to calculate strain. This allows numerous geological objects to be used for strain analysis using objective calculations developed for ellipse analysis.

Chapter 6, *Ellipse Data Graphs* covers graphical techniques for two-dimensional strain plots, including $R_f \phi$ graphs and polar Elliott graphs, which are types of *hyperboloidal projections*. Hyperboloidal projections are analogous to spherical projections, such as the stereographic and equal-area projections that are used to create stereonets and Schmidt nets respectively, familiar to students of structural geology.

Chapter 7, *Mean Ellipse Calculation*, discusses the calculation of a mean ellipse from a sample of ellipses. As discussed in Chapter 5, these calculations apply to polygons as well as ellipses, as the use of polygon moment equivalent it ellipses removes the requirement that particles were initially elliptical.

The techniques mentioned thus far are related to two-dimensional strain analysis. Chapter 8, *Ellipsoid Calculation*, covers the more complex steps involved in determining three-dimensional strain ellipsoids from oriented sections for which the two-dimensional strain ellipse has been determined. Chapter 9, *Ellipsoid Graphs*, covers strain graphs used to display this type of data, Flinn and Nadia graphs.

Chapter 10, *Data Transformation* discuses methods for transforming data sets, including *unstraining* or *retrodeforming* data sets and images to their pre-deformation state. Chapter 11, *Data Synthesis*, covers data synthesis for making artificial samples from random populations. Chapter 12, *Image Analysis* discusses image analysis techniques, including filtering and edge finding, that can aid in highlighting particle edges prior to digitizing.

 It is essential to be aware of the assumptions involved in strain analysis. Refer to the referenced texts for a complete discussion. An important consideration is whether the particles, such as fossils or clasts, record the same deformation as the rock. In general, this means whether there was a viscosity contrast between the particles and the matrix that encloses them. This is discussed briefly in Chapter 3.

A second problem to consider is whether there was an initial preferred orientation of the particles, this can be related to an initial sedimentary fabric, or compaction. Unimodal, or orthogonal, sedimentary fabrics and compaction essentially apply a "deformation" that is indistinguishable from a tectonic deformation without additional information. Detection of initial fabrics is discussed briefly in Chapter 7. Similarly, volume change is difficult to quantify, and strain is generally calculated with volume equivalent to an initial unit sphere.

This User Manual is written in a tutorial fashion, in order to become acquainted with the program, it is a good idea to work through the examples provided. This User Manual is also not yet finished, it is a work in progress.

3. Strain from Points

It is common in nature for objects to be distributed randomly, but with some minimum cutoff distance between them. A random distribution in space follows a *Poisson distribution* (see, for example, Davis, 1986), basically a distribution gotten by throwing pingpong balls randomly into an empty room. However the centers of the pingpong balls can never touch, giving a cutoff distance of twice the radius of the balls.

This distribution is called a *truncated Poisson distribution* (e.g., Shana and Xiao, 2011). Examples of this type of data include the centers of clasts in many sedimentary rocks such as sandstones and conglomerates. The centers of phenocrysts in igneous rocks, where nucleation of new crystals is prevented in proximity to existing crystals due to the chemical gradient, is another example. Note that if the particles have a different viscosity than the enclosing matrix, even if they are perfectly rigid, it is possible to get an estimate of the strain of the rock. Thus it is possible to extract different information than by an analysis of the particle shapes.

3.1 Fry Analysis

The basic idea for methods utilizing point distributions (e.g., Ramsay and Huber, 1983) is that the distance between the initial object centers is the same in all directions, and after a deformation the particles are closer in some directions and further in others. This new distribution will be elliptical in two dimensions, or ellipsoidal in three-dimensions. A *Fry analysis* (Fry, 1979) is an important and widely used technique for analyzing this type of data, and there is an extensive literature on it and its variations (e.g., Hanna and Fry, 1979; Crespi, 1986; Onasch, 1986; Erslev, 1988; Erslev and Ge, 1990; Dunne, Onasch, and Williams, 1990; McNaught, 1994; McNaught, 2002; Shan and Xiao, 2011; Waldron and Wallace, 2011; Mulchrone, 2013).

A Fry analysis can be simply done with two pieces of tracing paper, by tracing all of the particle centers on one sheet, then drawing a center point on a second sheet overlain on the first, and then sequentially moving the center point to each point and trace each point. For *n* initial points, this generates:

$$n_f = n! / (2 * (n - 2)!)$$

points, which is a lot of points to draw by hand. To illustrate the use of the method in EllipseFit, start EllipseFit and open the file (*File > Open*):

E2 - Ramsay and Huber 1983 (large).jpg

This is a photograph of a deformed ironstone oolith in thin section from Ramsay and Huber (1983) that is widely used as a test image for strain analysis. For point digitizing make sure the red *Point Icon*

(second from left) is displayed (*Digitize > Center Point*), and the green *Plus Icon* is selected (*Digitize > Add Tool*), as in Figures 1 and 2.

Use the zoom tools to enlarge the image, and click on one particle center. The *Data Window* will open and display a highlighted line of data. Before continuing, open the Fry graph (*Analyze > Fry Graph*). You should have something similar to Figure 2.

Figure 1. EllipseFit's Image Window used for digitizing, with photomicrograph of a deformed oolite from Ramsay and Huber (1983).

Continue digitizing point centers, you should ideally work out from one point digitizing adjacent points keeping a roughly circular area. The Fry graph will start to develop as you digitize, with each new set of generated points highlighted (Figure 3).

Use the *Hand Tool* (*Digitize > Hand Tool*, or the *Hand Icon*) to scroll, and the Zoom Tool to zoom (*Digitize > Zoom* or the *Magnifying Glass Icon*). You can also use the Command (Mac) or Control (Windows and Linux) + and – keys to zoom in and out. Holding down the Shift key allows scrolling with the cursor. Points can be deleted by using the *Find Tool* (*Digitize > Find Tool* or the *Binoculars Icon*) to highlight a point, and delete it using the *Cut* command (*Edit > Cut*) or red X icon. A point can also be deleted by selecting it in the Data Window and deleting it there.
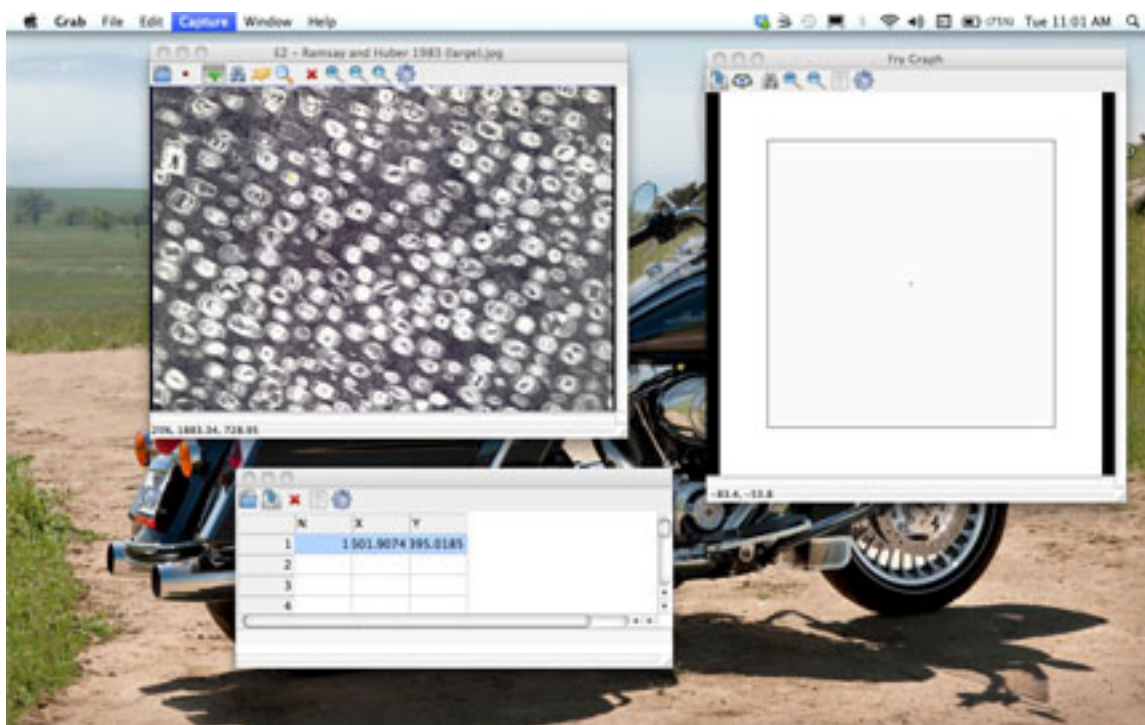
Figure 2. EllipseFit's *Image Window*, *Data Window* and *Fry Graph* displaying a single data point.

It is important to be objective, and you may wish to digitize all available points, however note that some particles may not meet the required assumptions. In particular, note that the centers of the particles in two-dimensions do not generally correspond to their three-dimensional centers, as they lie on an arbitrary plane cutting through the rock, so the assumption of of a uniform cutoff is weakened. This is discussed further in Section 3.2, Normalized Fry Analysis.

Additionally, it is desirable to select approximately equal numbers of particles in all directions, so the point density is not biased by direction. This is one reason to maintain a uniform point density in a circular area while digitizing, and why having the interactive Fry graph open can assist in particle selection. This is discussed further in Section 3.2, Mean Log Likelihood Function (MLLF).
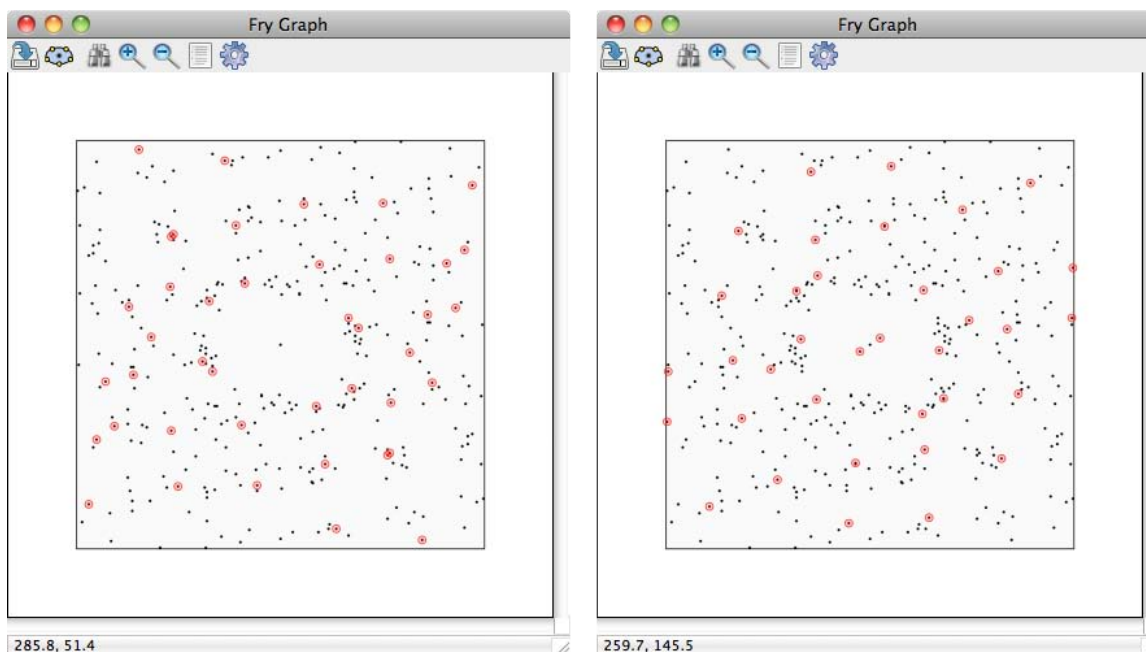
Figure 3. Fry graph after digitizing 20 adjacent particle centers. The generated points are highlighted. On the right, note the presence of the spurious data point (each point is mirrored about the center) generated by clicking too close to an existing point, i.e. an operator error which can be deleted.

If you wish to change the size of the digitized points, click the *Gear Icon* (or *Preferences*) from which you can set most of the EllipseFit preferences. Note some selections have multiple pages, use the left-right arrows (*Command < >*) to go through them. You can preview the effect of preference changes before setting then with the *OK* button.

To view the data as a *Strain Map* select *Analyze > Strain Map*. This displays the data as particle centers, this population can be strained and unstrained as described in Chapter 10, Data Transformation.
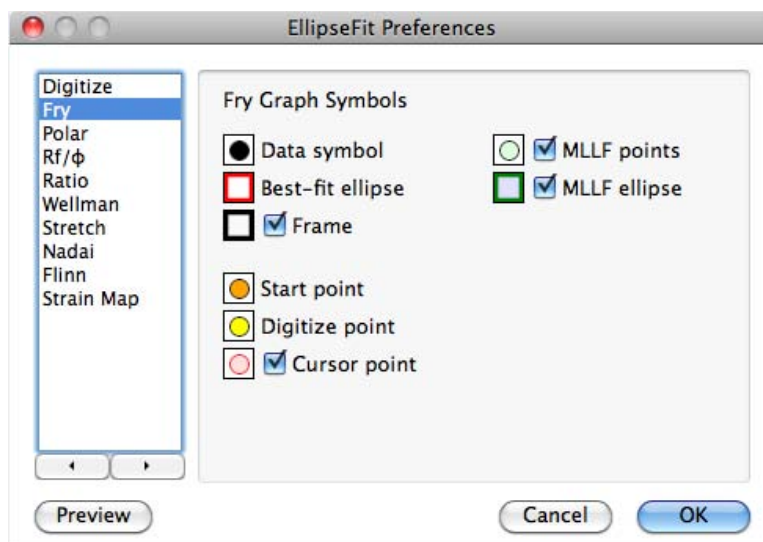

Figure 4. The EllipseFit *Preferences Dialog* where most preferences are set. Note the left-right arrows used to scroll to additional pages if present.

Figure 5 is the graph after carefully selecting 60 particle centers, a probable minimum number for analysis (Shan and Xiao 2011), and after digitizing 252 points, essentially all of them.
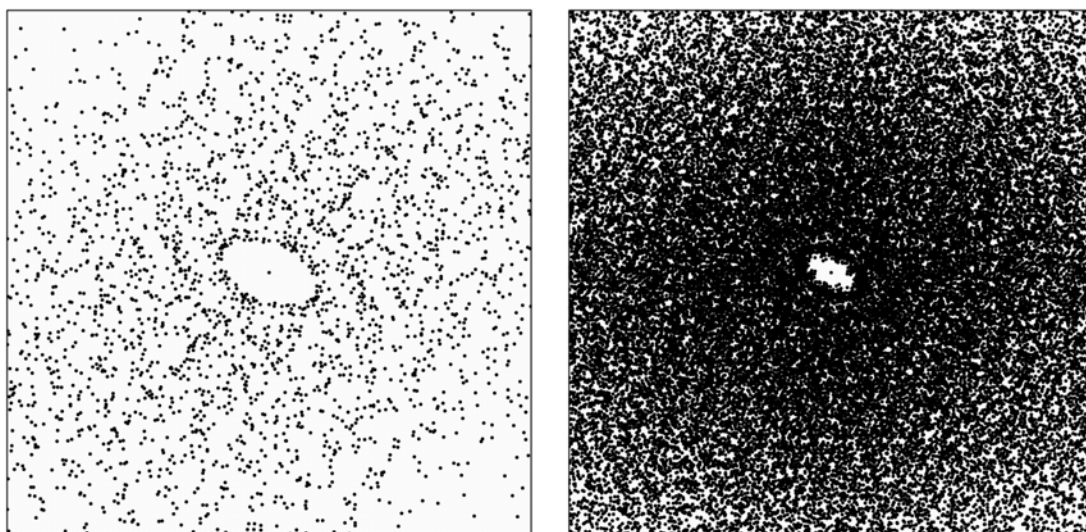

Figure 5. Fry graphs after digitizing 60 carefully selected points, and after digitizing 252 points, essentially all of them. These images are PNG files as saved from EllipseFit.

To zoom in for a better image of the central void, open the *Preferences Dialog* (*Gear Icon*), uncheck *Auto-scale,* and enter a number smaller than the displayed *Data radius* (Figure 6).
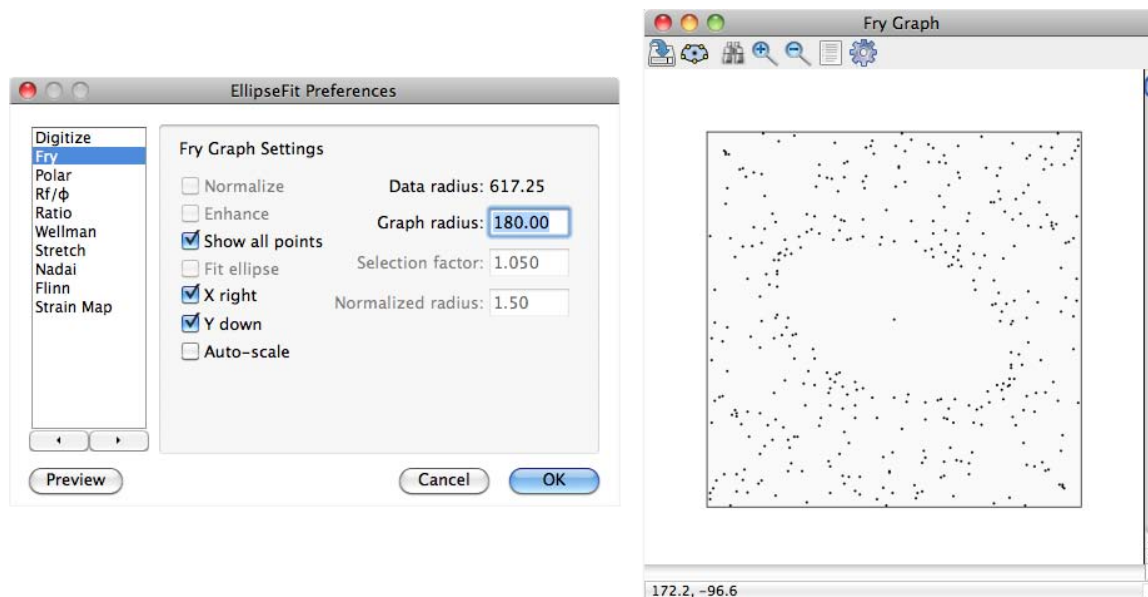

Figure 6. Set the graph radius to display the central void by unchecking Auto-scale, and entering a smaller radius.
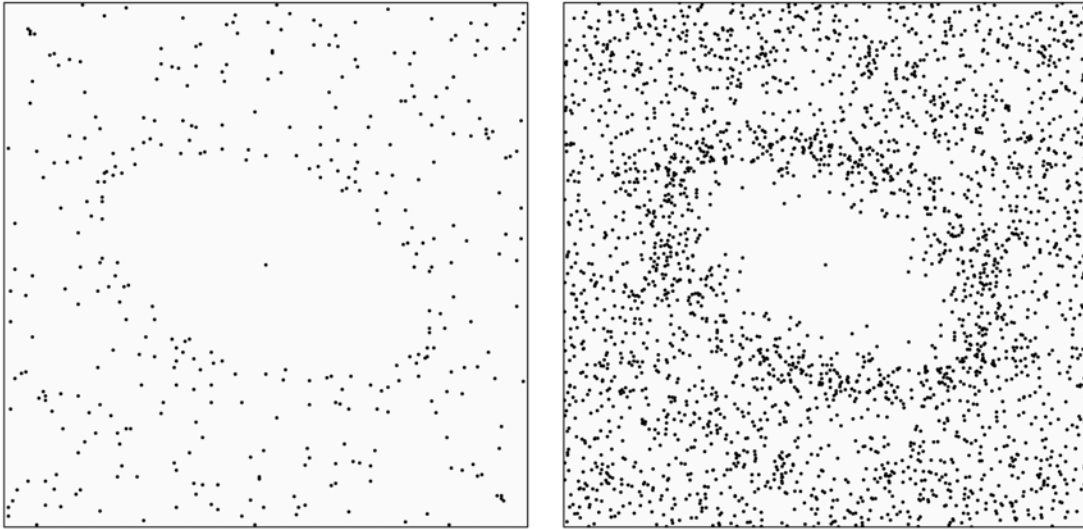
Figure 7. Close up of the central voids for the two data examples of 60 and 252 points.

Figure 7 shows the zoomed in central voids for the two examples. The next step is to determine the *best-fit* ellipse for the central void displayed in Figure 7. This can be a subjective process, and objectively choosing this ellipse is the subject of a number of papers (e.g, Erslev, 1988; Erslev and Ge, 1990; Shan and Xiao, 2011; Waldron and Wallace, 2011; Mulchrone, K.F., 2013).

The *normalized* Fry method (Erslev, 1988; Erslev and Ge, 1990) is one that is commonly employed, but requires the digitized ellipses of each particle. The normalized Fry method is the subject of Section 3.2.

Ideally a method should require only the point data (e.g., Shan and Xiao, 2011; Waldron and Wallace, 2011; Mulchrone, K.F., 2013). Currently EllipseFit implements the algorithm of Shan and Xiao (2011), discussed in Section 2.3.

For the purposes of this section, it will be assumed that the void has been defined well enough to pick out the void by eye, which may be a close enough estimate, and also makes a good exercise for introductory students.

Click on the Centered Ellipse Icon (*Digitize > Centered Ellipse*), and click at the edge of the void. An orange circle marks the starting point, subsequent points are marked by a yellow circle. When finished, click on the orange circle and the ellipse will be calculated and displayed in the Log Window.
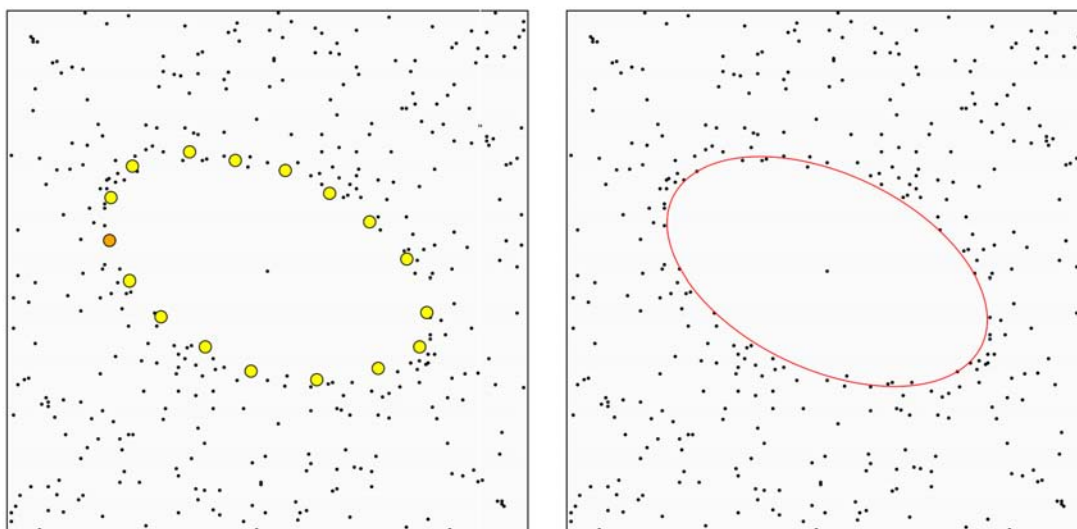
Figure 8. Digitizing the central void. The orange point is the start point, the yellow are subsequent points. Click on the orange point when finished, and the ellipse is calculated. The point size is set larger than the default size for the illustration.

For this sample, the calculated results are reported by EllipseFit as:

```
N = 60
Pairs = 1770
Best-Fit Ellipse
  Manual
  n = 17
  R = 1.758
  Φ = 25.45°
  RMS = 0.0583
```

A centered ellipse was calculated from the 17 digitized points. The calculation is rotationally invariant, and the best fit found by minimizing the sum of the squares of the distance of the points from the ellipse, i.e., the *residuals*. The minimization is solved from the linear equations using a LU decomposition.

The RMS value is the *root mean square* measure of the variation of the residuals from the ellipse, that is the square root of the sum of the squares of the residuals of the data from the fitted ellipse. RMS is a common way to express goodness of fit of least squares solutions. It is not a measure of the error in the strain calculation, and is not technically an error. It is, however, a measure of how closely the digitized points fit the ellipse. A small RMS means that the entered points lie close to an ellipse. It makes a good class exercise for students to solve and compare their results and RMS.

As a final step in this analysis, select the *Edit > Transform Image* command and enter the results into the dialog as in Figure 9. The image will be unstrained to remove the calculated strain as shown in Figure 10.
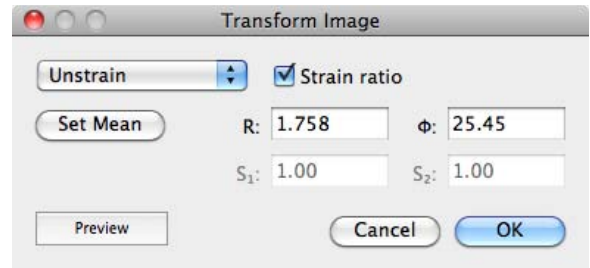

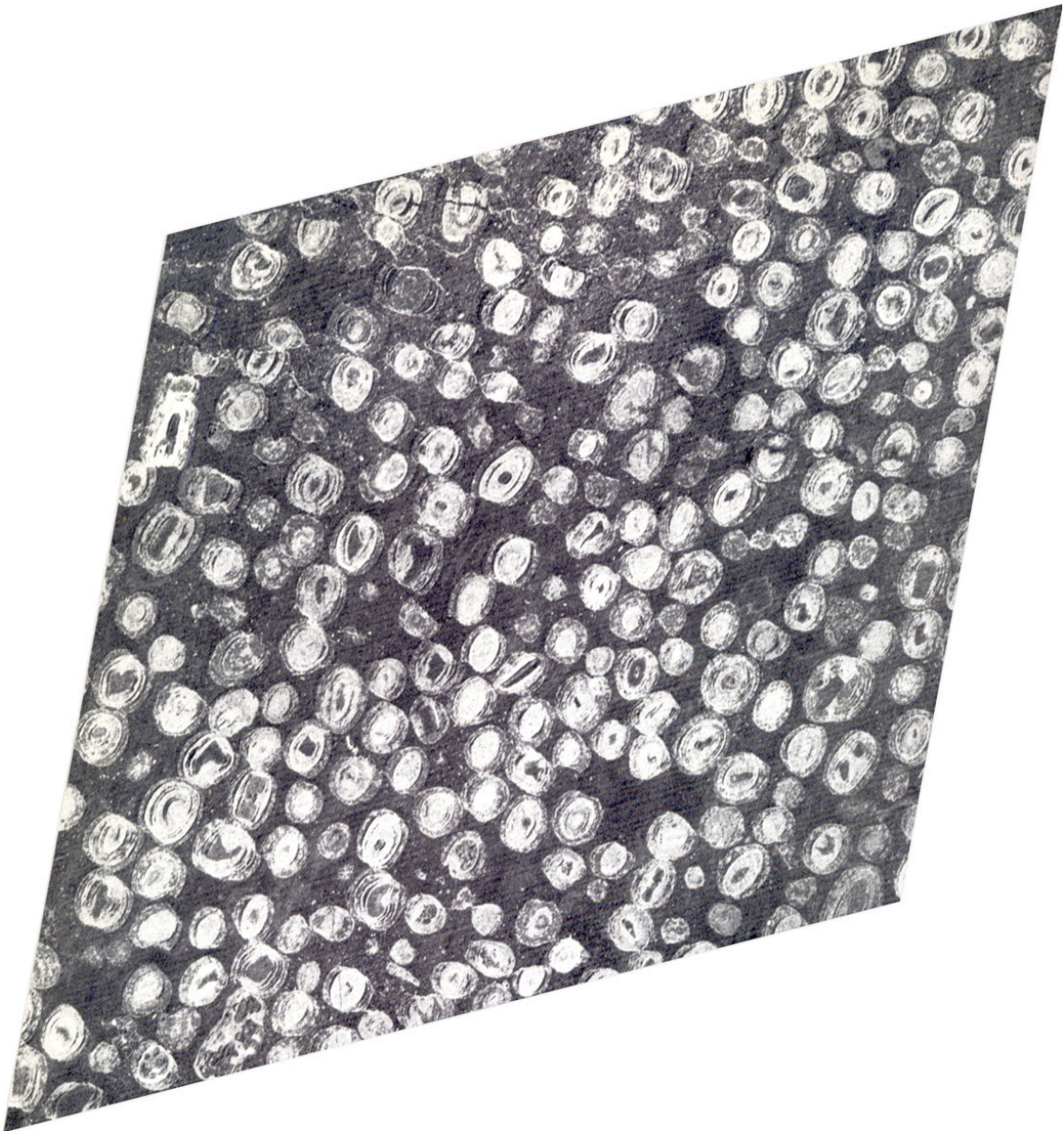Figure 9. The *Transform Image* dialog with values entered to unstrain the mage.

Figure 10. The oolith photomicrograph after being unstrained using EllipseFit's Image Transform command.

Next select the *Analyze > Transform Data* command and enter the calculated values as shown in Figure 11. Press *Transform* and then *Accept*.
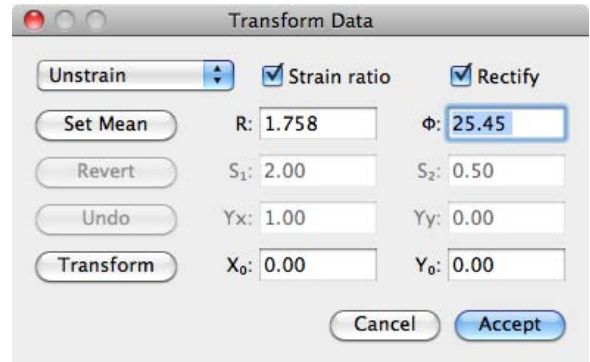

Figure 11. The Transform Data dialog with values entered to unstrain the data. *Set Mean* is only used with ellipse data. *Rectify* resolves the offsets caused by the image transformation.

The data is unstrained using the calculated values, as shown by the Fry graph in Figure 12. The *Rectify* option resolves the offsets caused by the image transformation, so the data points remain centered over the particle centers.
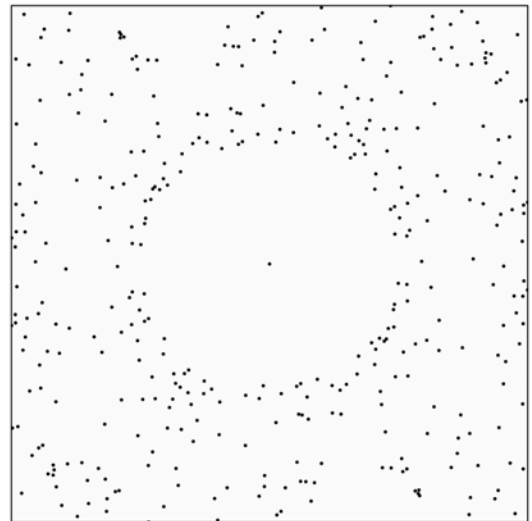

Figure 12. Fry graph of the unstrained 60 point data after using the *Transform Data* command to unstrain (retrodeform) the data using the calculated values.

3.2   Normalized Fry Analysis

As discussed in Section 3.1, the Fry analysis is a two-dimensional solution to a three-dimensional problem, since initial particles are assumed circular instead of spherical. Even if the particles have a uniform size, a section through a sample will show them as different size particles. One solution developed to overcome this is the *normalized Fry* analysis (Erslev, 1988; Erslev and Ge, 1990 McNaught, 1994; McNaught, 2002).

The distances between particles are *normalized* to account for the difference in the sizes of the particles, which can greatly improve the sharpness of the central void. Unfortunately, the ellipse sizes and orientations are required for this, and in most cases if the ellipse data is available, it should used for the strain analysis following techniques in Chapter 7, Strain from Polygons. However, as mentioned in Section 3.1, a Fry analysis can provide different information regarding particle versus matrix strains.

The digitizing of ellipses is discussed in Chapter 5, Strain from Ellipses, so for an example of this analysis, open the image file:

   E2 - Ramsay and Huber 1983 (small).jpg

and the data file:

   E2 - Ramsay and Huber 1983 (small)

This is the 252 point data set used in Section 3.1.

The data is overlain on the image, and, if the *Binoculars Icon* is selected, you can select individual particles that are highlighted in the *Data Window* and the *Fry Graph*. This selection method is implemented for most of the graphs discussed in subsequent chapters. The Fry graph will look like Figure 5B.
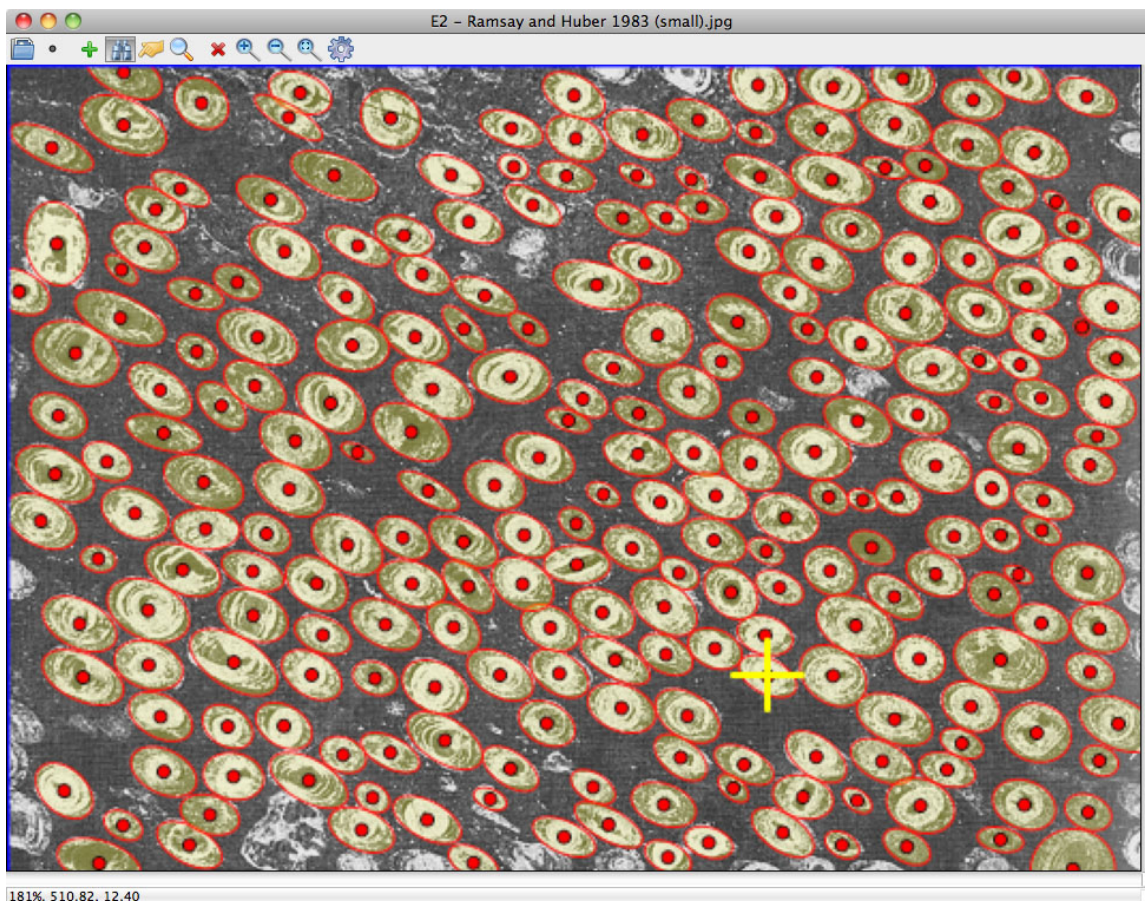
Figure 13. EllipseFit Image Window with ellipse data overlain. Selecting the *Binoculars Icon* (as shown) allows interactive selectiin of particles that are highlighted in the Data Window, as well as on data graphs including the Fry Graph.

To zoom in on the central void, open the *Preferences* dialog (*Gear Icon*), deselect *Auto-scale*, and enter 50 for the *Graph radius* as shown in Figure 14.
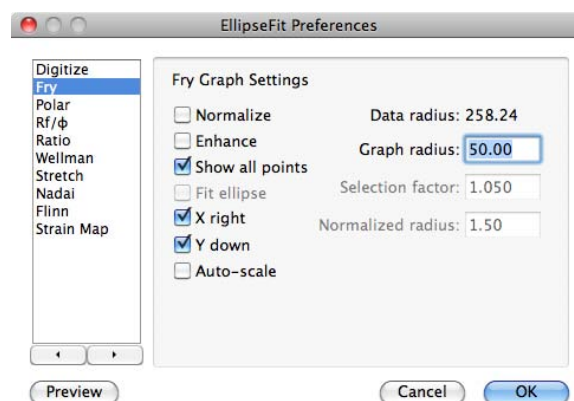
Figure 14. Settings to display the central void without normalizing.

The unnormalized graph is displayed in Figure 15.

Figure 15. The Fry graph without normalizing, using the settings displayed in Figure 14.

To normalize the graph select *Normalize,* as shown in Figure 16. Note that the *Normalized radius* is now used due to the normalization to a unit circle, the default value is 1.5 as shown.

Figure 16. Settings to display a normalized Fry graph. Note that the Normalized radius is now used due to the normalization to a unit circle.

The resulting normalized graph is shown in Figure 17. Note the clear sharpening of the central void.
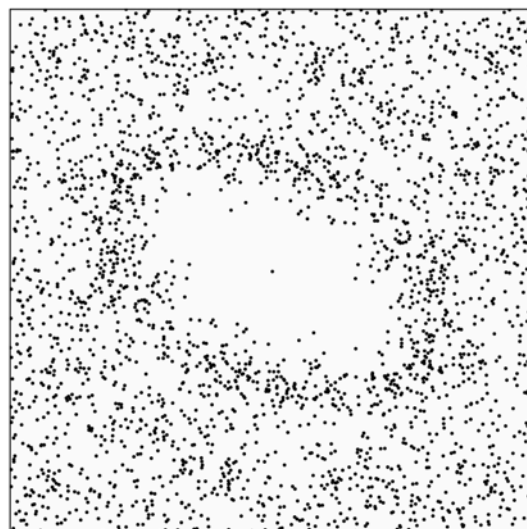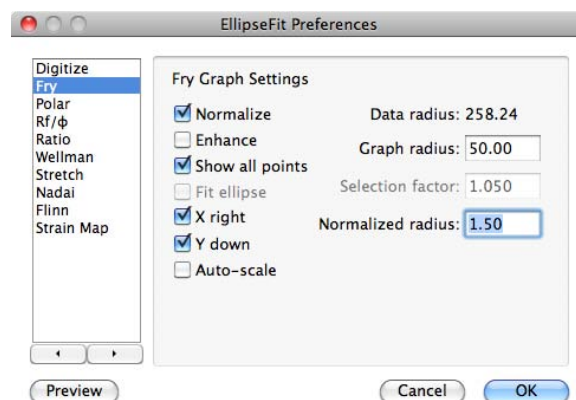
The final question addressed in his section is how to find the ellipse corresponding to the central void. The *enhanced normalized Fry* method (Erslev and Ge, 1990) uses a user specified cutoff radius to exclude particles beyond the a certain distance from the void center. This is a subjective value, chosen here with a default value of 1.05. In the *Preferences* dialog check *Normalize*, and uncheck *Show all points*. EllipseFit calculates the best-fit ellipse through the cloud of points using the least squares method described in Section 3.1.
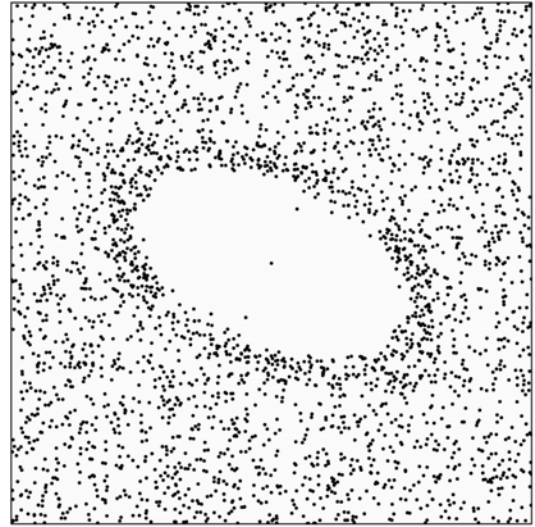
Figure 17. Graph of the normalized data. Note the better resolution of the central void.

The results from the *Log Window* are:

```
N = 252
Pairs = 31626
Normalized
Enhanced
Selection factor = 1.050
Enhanced pairs   = 142
Best-Fit Ellipse
  Automatic
  n = 142
  R = 1.581
  Φ = 24.46°
  RMS = 0.1383
```
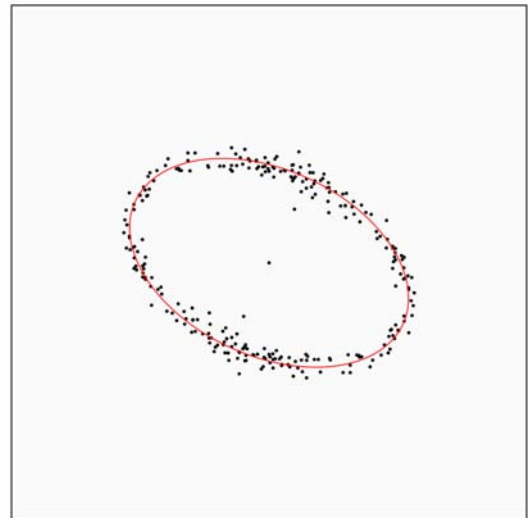

Figure 19. Fry graph with ellipse fitted to the enhanced normalzed points.

Again, the RMS is a measure of the deviations of the residuals, and can be used to refine the selection factor. However, note that smaller number of points will generally have a smaller RMS. For example three points give RMS = 0, so finding the minimum RMS is not a valid strategy.

Section 3.3   Mean Log Likelihood Function (MLLF)

Calculating the strain from a sample of points should ideally require no additional information about the particle's shapes, and there are a number of methods that have been developed for this purpose (e.g., Shan and Xiao, 2011; Waldron and Wallace, 2011; Mulchrone, 2013). EllipseFit implements the *mean log likelihood function (MLLF)* method of Shan and Xiao (2011). They examine the statistics of a truncated Poisson distribution, and define the MLLF as the average sum of the log probability distribution function (PDF) of each individual point in the deformed state. This is related to the density distribution around each point.

The PDF in the deformed state is related to the pre-deformation PDF by the shape and orientation of the central void, giving as parameters a cutoff distance, the ratio R, and the orientation Φ. The function is complex however, and is solved using a gird search to locate the maximum MLLF. The search is over the range $\Phi = 0°$ to 179° in steps of 1°, and R = 1 to 20 in steps of 0.1. The latter value is the default that can be changed if desired, a smaller value will speed up the search. Once R and Φ are determined, the sample is retro-deformed, and a 50 step search is done to locate the cutoff radius.

Shan and Xiao (2011) further suggest an approach to improve the results using a cross validation technique for detecting spurious points by sequentially removing up to 10 points, the default value in EllipseFit, and repeating the search. These algorithms were implemented by Y. Shan in a Fortran program which he provided, EllipseFit has been carefully tested to insure that identical results are obtained.

The result are the best estimates values of R, Φ. initial cutoff distance, and a set of neighborhood points. This method has advantages in that it is a robust numerical solution, and one that uses all of the points to define the central void. In comparison, the enhanced normalized Fry method that only examines the points close to the void.

A disadvantage of the method is the computing time required to calculate the solution. In particular the cross-validation can take several hours. Shan and Xiao (2011) also note, wryly, that it is a pity that the treatment does not require the Fry plot, which will disappoint structural geologists who prefer manual manipulation and visual appreciation. To assist, I have tried to make the output plot as visually pleasing as possible.

To run a test sample open the file MLLF Test 60.csv. This data is the 60 point oolth sample used in section 3.1, and was carefully selected to avoid spurious points, and to avoid a directional bias.

Select the command *Analyze > Calculate Ellipse*. Note that the only available options are the MLLF options, the other options all require ellipse data. Select *Mean log likelihood*, leave *Cross validate* off as in Figure 20, and press *OK*.

A progress dialog will appear as in Figure 21, the display shows the search iteration passes in degrees, and is done at 180. The process should complete in less than a minute, and the results displayed in the Log Window, and on the Fry graph (Figure 22).

Figure 20. The *Calculate Ellipse* dialog showing the MLLF options available for a set of point-only data.

Figure 21. Progress dialog for the MLLF grid search without cross validation.

The results reported in the log file are:

```
N = 60
MLLF Calculations
-----------------
Pass    Mean LL      R    Phi     Cutoff        Stat    Density
   0   -0.31829   1.90  25.00   86.98953     0.67361    0.84687
MLLF Results
-----------
Point statistics:
Number                        =          60
Calculated density            =     0.00004
Real density                  =     0.00000
Results:
Mean log-likelihood           =    -0.31829
R, strain ratio               =     1.90000
Phi, angle of max strain axis =    25.00000
Cutoff radius                 =    86.98953
```

Figure 22. Fry graph with results of the mean log likelihood function (MLLF) maximization search. The ellipse is the result of the MLLF grid search. The green markers highlight the Fry neighbor points.

The Fry graph of the mean log likelihood function (MLLF) maximization search results is shown in Figure 22. The ellipse is the result of the MLLF grid search. The green markers highlight the Fry neighbor points, those that maximize the MLLF. Note the ellipse is the result of the intensive grid search, and is not simply a linear least squares fit as used in Sections 3.1 and 3.2.

To test the cross validation procedure, go back and check the *Cross validation* option in the *Preferences* dialog. The progress dialog now is displayed as in Figure 23. There are now three iteration passes displayed, the first is 0 to 10, where 0 is the first calculation as done above. Passes 1 to 10 are the cross validation iterations, 1 to 60 are the data points, and 1 to 180 are the Φ grid search in degrees. The R grid search values (0.1 to 20.0 by default), and the 1 to 50 distance search loops are not displayed.

The MLLF search is computationally intensive, especially for cross validation (during some test runs I set my laptop on marble coasters to keep it from overheating). After about 6 hours (on a 3.06 GHz Intel Core 2 Duo iMac) the process completes, and the dialog displays *OK*. You can cancel the run at any time, and the results of the completed passes will be displayed.
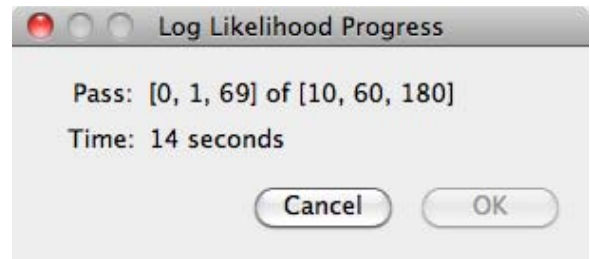
Figure 23: Progress dialog for the MLLF grid search with cross validation.
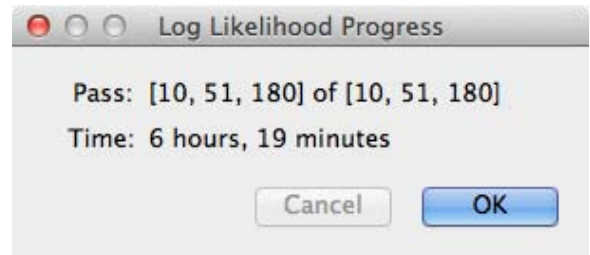
Figure 24: Progress dialog for the MLLF grid search with cross validation when complete.

```
Mean Ellipse Calculations
MLLF Test 60.tsv
2014-05-31 16:30:46
==============================
N = 60
MLLF Calculations
-----------------
Pass    Mean LL      R    Phi     Cutoff       Stat      Density
   0    -0.31829   1.90  25.00   86.98953    0.67361     0.84687
   1    -0.31610   1.90  25.00   86.98953    0.68773     0.86122
   2    -0.31603   1.90  25.00   86.98953    0.69522     0.87607
   3    -0.31882   1.90  25.00   86.98953    0.67496     0.89144
   4    -0.31651   1.90  25.00   86.98953    0.68968     0.90736
   5    -0.31536   1.90  25.00   86.98953    0.70494     0.92386
   6    -0.32428   1.80  23.00   87.24708    0.68393     0.93542
   7    -0.31554   1.90  25.00   86.98953    0.69945     0.95872
   8    -0.31327   1.90  25.00   86.98953    0.71578     0.97716
   9    -0.31454   1.80  23.00   87.24708    0.69591     0.99044
  10    -0.31451   1.90  25.00   86.98953    0.69099     1.01624

MLLF Results
------------
Point statistics:
Number                              =         52
```

```
Calculated density                 =      0.00004
Real density                       =      0.00004

Results:
Mean log-likelihood                =     -0.31327
R, strain ratio                    =      1.90000
Phi, angle of max strain axis =         25.00000
Cutoff radius                      =     86.98953

Finished: 2014-05-31 22:49:58
```
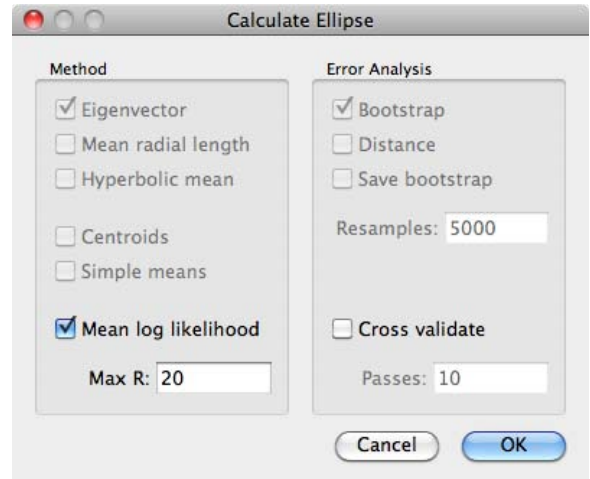
The results of pass 0 are identical to the previous result, however the cross-validation procedure located a slightly better solution, in pass 8 the mean log likelihood is -0.31327, instead of -0.31829. The resulting Fry graph with 8 less neighbor points is shown in Figure 25.
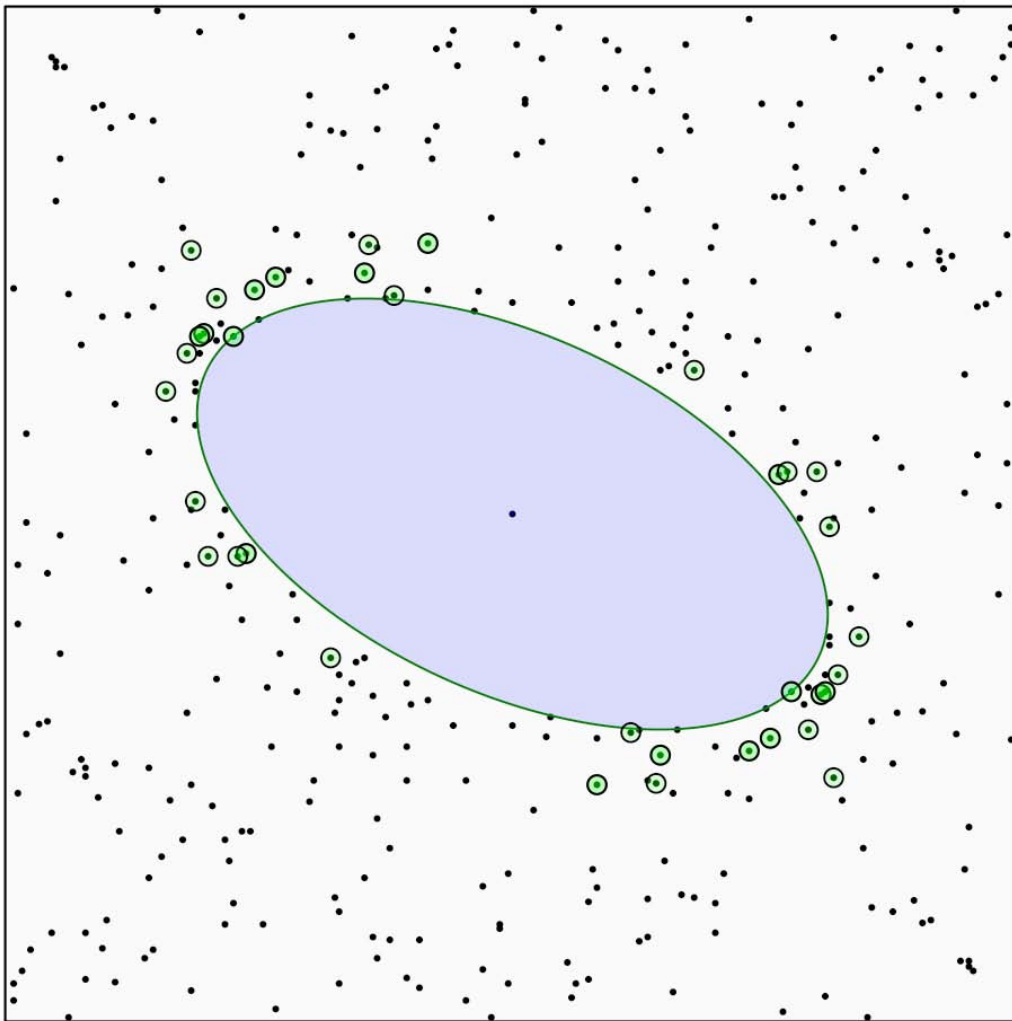

Figure 25: Fry graph of the results using the cross-validation option for mean log likelihood maximization.

4.   Strain from Lines

[Documentation in preparation]

4.1   Analytical Wellman Analysis

The Wellman method can be applied to objects in which *two lines* can be identified that have *constant initial angles*, such as brachiopod hinge and medial lines which are initially perpendicular (Wellman, 1962; Ramsay, 1967). For brachiopods not parallel to a principal strain, this angle will be distorted by shear strain.

Wellman's graphical technique is illustrated in many structural geology laboratory manuals (e.g., Ragan, 2009). An analytical solution to the problem was given by Vollmer (2011), which is implemented in implemented in EllipseFit. To try the method, open the file

>   LA - Ragan 1985 F10_1a.png

as an image. This is from Ragan (1985), and is used in many structural geology classes as an exercise. To begin click on the digitizing icon at, the second from the left, until the LinePair Icon is displayed, or from the menu choose *Digitize Line Pair*. Click on the endpoints of each of the two lines in turn. When done the lines appear in red, and the yellow cursor appears at the intersection. Mistakes can be corrected by using the red X *Cut Icon,* or by deleting the line pair in the *Data Window*.
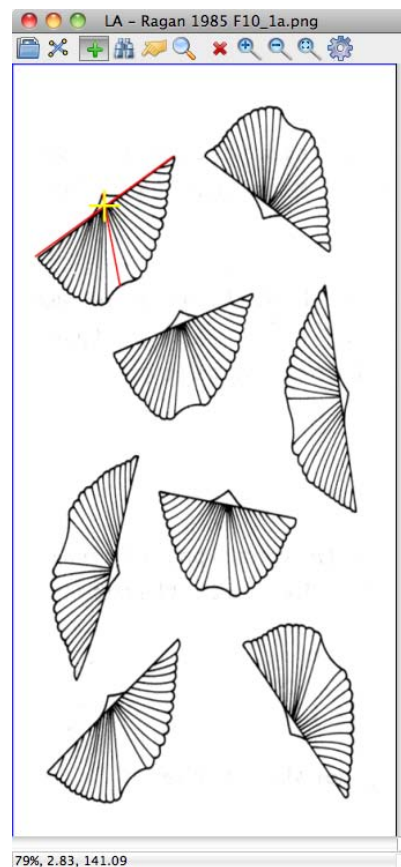

Figure 26: The Image Window after opening the example data for the analytical Wellman method from Ragan (1985). The hinge and medial lines are assumed initially perpendicular. One line pair has been digitized.Note the *Line Pair Icon* is visible.

After digitizing one line pair, open the Wellman Graph using the menu command *Analyze > Wellman Graph*. The graph shows the parallelogram corresponding to the brachiopod (Figure 27). The parallelogram sides parallel the line pair. Note the two additional points used for the construction.
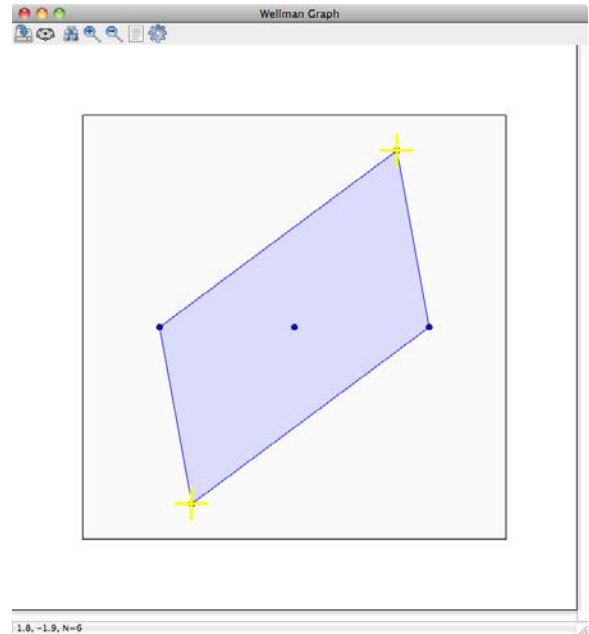
Figure 27: The analytical Wellman graph diplayed in a graph window after digitizing one line pair as in Figure 26. Note the Binoculars Icon is selected and that the parrallelogram and corresponding brachiopod are selected with the yellow cursor.

Continue digitizing the remaining line pairs. Figure 28 shows the graph after three line pairs. The yellow cross cursor highlights the corresponding data point intersection and parallelogram, and the data is selected in the *Data Window*. If the *Binoculars Icon* is pressed, as in Figure 28, you can search on the graph to locate the corresponding data. As in digitizing points, this allows the identification of outliers or spurious data.

Figure 28: The analytical Wellman graph after three line pairs have been digitized.

Figure 29: The final analytical Wellman graph after all 8 line pairs from the brachiopods in Figure 27 have been digitized.

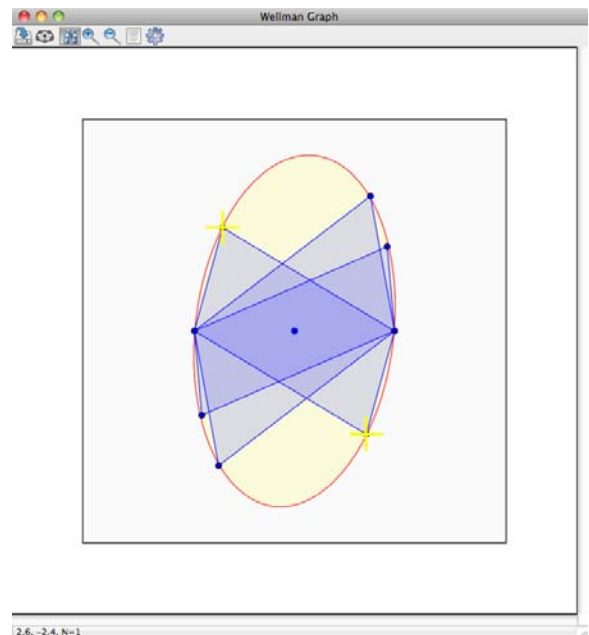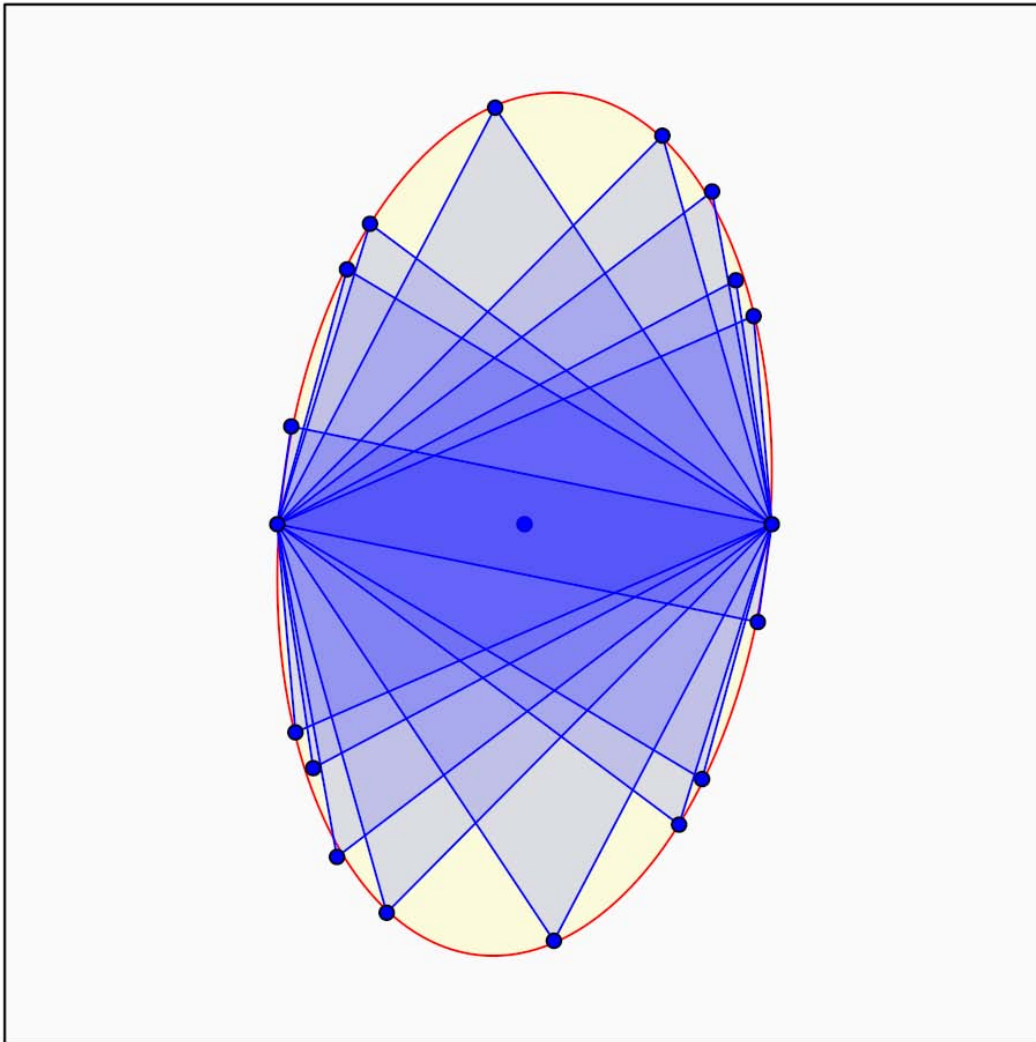Figure 29 shows the final analytical Wellman graph after all 8 line pairs have been digitized. Examine the *Log Window* (*Window > Log*) and note that at each step EllipseFit calculated the best-fit ellipse.

```
Analytical Wellman Ellipse Results
Wellman Data.tsv
2014-06-01 21:39:47
==============================
N           = 8
Point pairs = 9 (symmetric)
R           = 1.773
Φ           = 96.10°
n           = 9
RMS         = 0.025
```

The calculation is the same as described in Sections 3.1 and 3.2, minimizing the sum of the squares of the residuals the points from the ellipse using a LU decomposition. Similarly, the RMS value is the *root mean square* measure of the variation of the residuals from the ellipse, that is the square root of the sum of the squares of the residuals of the data from the fitted ellipse. It is a measure of goodness of fit of the ellipse, but is not technically an error. The RMS will be zero for two line pairs. The calculation includes the constriction line, so the ellipse has 9 point pairs including the 8 data points.

In theory, objects like graptolites that have a constant, non-perpendicular, angle between stipe and thecae, can be treated in the same fashion (Ramsay, 1967). Dirringer and Vollmer (2013) compared the automated Wellman method and the *mean polygon moment ellipse* method (Section 5.1) using a sample of slate with deformed Ordovician graptolites. The sample was oriented with the slaty cleavage as the X axis. The center lines and lower thecae lines were digitized in 120 locations for the Wellman test, only one species had clearly defined thecae lines. The outlines of 31 whole graptolites and 38 partial graptolites were digitized for the polygon method test.

The *mean polygon moment ellipse* was R = 2.079 ± 0.122, Φ = 177.48° ± 4.57°, parallel to the slaty cleavage. The polygon method does not require assumptions about initial shapes, only that they are initially random. Interpreting the data for the analytical Wellman method was problematic, as it many outliers around a central ellipse. Removal of 77 outliers, believed to be due to initial variations in thecae angle, was required before the ellipse could be clearly resolved. While most outliers could be clearly identified, the process was subjective, and single outliers significantly effected the result. The result for 43 data points was R = 2.761, Φ = 0.50°, RMS = 0.294, parallel to cleavage.

They concluded that the necessary assumptions about initial geometry for the analytical Wellman method were not met, and the polygon method, with no such required assumptions about initial geometry, was preferred.
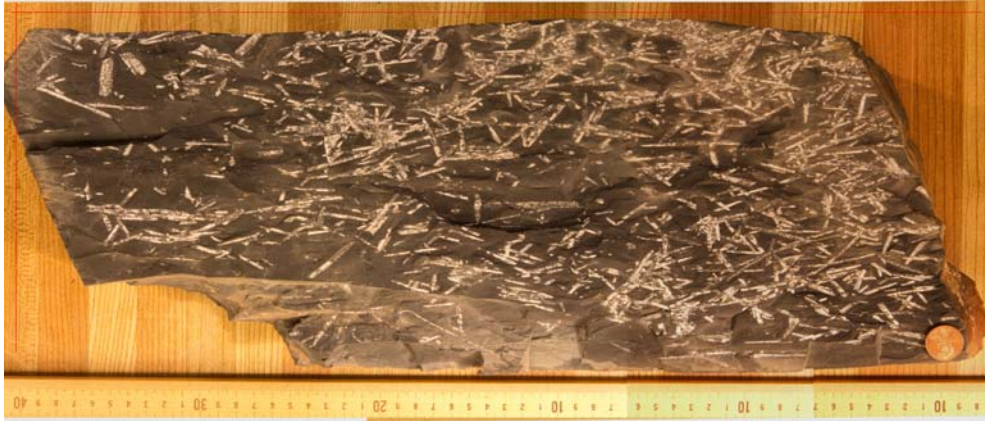
Figure 30: Sample of deformed graptoliferous slate used by Dirringer and Vollmer (2013) for comparison of the automated Wellman and mean polygon moment ellipse methods.

Figure 31: The graptoliferous slate sample of Figure 24 after retrodeforming to remove the strain calculated by the mean polygon moment ellipse method, R = 2.079, Φ = 177.48°

4.2   Line Stretch Analysis

[Documentation in preparation]

5.   Strain from Ellipses and Polygons

[Documentation in preparation]

5.1   Digitizing Ellipses

[Documentation in preparation]

5.2   Moment-Equivalent Polygons

[Documentation in preparation]

6.   Ellipse Data Graphs

[Documentation in preparation]

6.1   Elliott Polar Graph

[Documentation in preparation]

The polar Elliott graph (Elliott, 1970) is a polar plot of the natural log R and 2ϕ. This is a natural parameter space for strain, and the grapg is a simple hyperboloidal projection that gives an undistorted representation (Yamaji, 2008; Vollmer, 2011), It is therefore generally preferred over the R_f ϕ graph of the next section.

Most of the graphs in EllipseFit are interactive. When the *Binoculars Icon* is selected, points can be selected and the selection will automatically update on other graphs and in the *Data Window*.

To illustrate, Figure 33 shows a Fry graph with the points generated by the outlier selected in Figure 32.

Figure 32. Polar Elliot graph with digitized data from the oolith photomicrograph in Figure 1. One outlier is selected.

Figure 33. Fry graph with data generated from the oolith photomicrograp in Figure 1. The selected points are those generated by the outlier selected in the polar graph of Figure 32

This outlier falls well inside the central void, and probably does not meet the assumptions necessary for a Fry analysis, i.e., a truncated Poisson distribution.

6.2   R_f ϕ

The R_f ϕ graph Dunnet, 1969) is probably more widely recognized and used than the polar Elliott graph (e.g., Lisle, 1985), however it distorts the strain space, especially at low strains, and a polar graph is generally preferred (Vollmer, 2011).
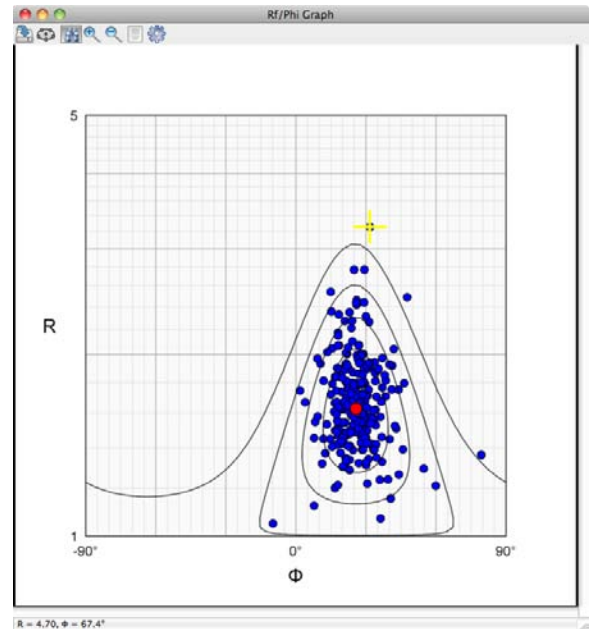
Figure 34. R_f ϕ graph with digitized data from the oolith photomicrograph in Figure 1. One outlier is selected, the same as in Figures 32 and 33, all of which are automatically updated interactively.

6.3   Hyperboloidal Projections

[Documentation in preparation]
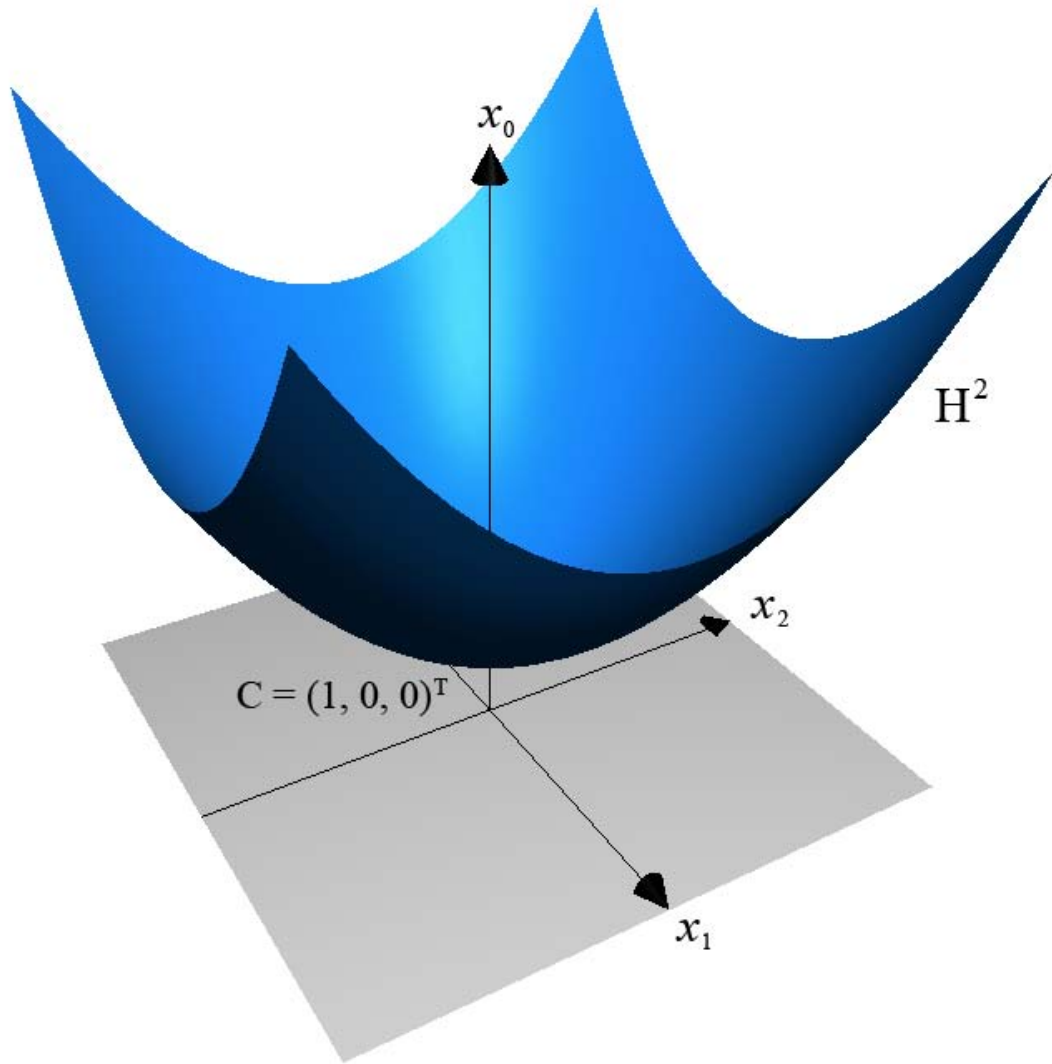
Figure 35: The unit hyperboloid, H^2, showing cartesian axes, x0, x1, x2, and point C = (1, 0, 0), which corresponds to the circle R = 1. The plane $x_1 x_2$ is the projection plane for azimuthal projections, the polar strain graph. Points on H^2 are $x = (x_0, x_1, x_2)^T$, with origin C. If strain is represented by $(\rho, \psi) = (\log R, 2\phi)$, then an ellipse is $x = (\cosh \rho, \sinh \rho \cos \psi, \sinh \rho \sin \psi)^T$
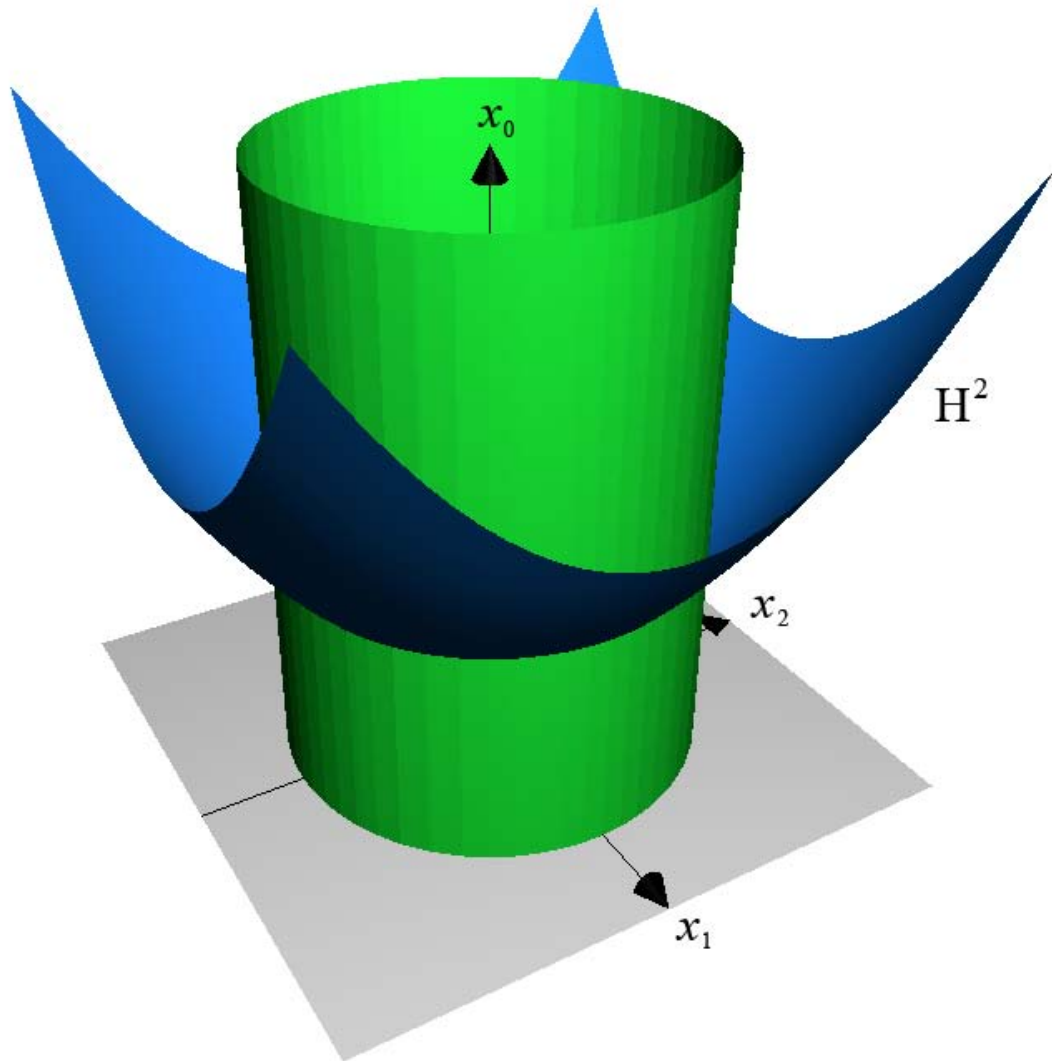
Figure 36: The unit hyperboloid with superimposed cylinder with axis x0. The cylinder is the projection surface for cylindrical projections, as the R_f ϕ graph.
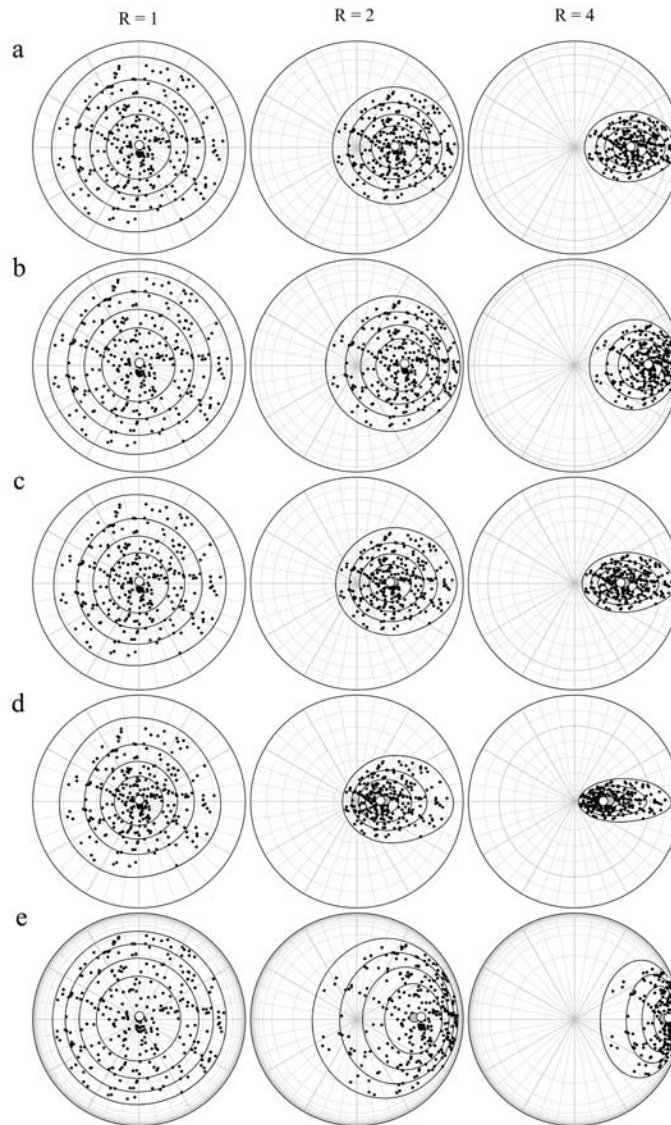
Figure 37. Synthetic data of 300 ellipses strained to values of R = 2 and R = 4 displayed on hyperboloidal azimuthal projections: (a) equidistant, (b) stereographic, (c) equal-area, (d) orthographic, and (e) gnomic.The best-fit ellipse is plotted as a white circle, the centroid of the projected data is plotted as a gray circle.

7.   Mean Ellipse Calculation

[Documentation in preparation]

Data Set	Imposed (R, φ)	Eigenvector	Mean Radial	Hyperbolic
Oolith	1, 0	1.628, 25.74	1.628, 25.74	1.628, 25.74
n = 252		± 0.018, 0.73	± 0.018, 0.62	± 0.013
	0.614, 25.74	1.000, 113.32	1.000, 113.32	1.000, 113.32
		± 0.007, 55.27	± 0.011, 633.74	± 0.013
Synth 1	1, 0	1.031, 40.20	1.031, 40.20	1.031, 40.20
n = 300		± 0.021, 33.24	± 0.025, 22.81	± 0.030
	2, 0	2.012, 1.16	2.012, 1.16	2.012, 1.16
		± 0.048, 1.16	± 0.050, 0.92	± 0.032
	4, 0	4.023, 0.46	4.023, 0.46	4.023, 0.46
		± 0.101, 0.53	± 0.099, 0.37	± 0.031
Synth 2	1, 0	1.016, 146.03	1.016, 146.03	1.016, 146.03
n = 1000		± 0.012, 35.35	± 0.014, 24.51	± 0.016
	2, 0	2.012, 179.46	2.012, 179.46	2.012, 179.46
		± 0.026, 0.71	± 0.27, 0.51	± 0.016
	4, 0	4.024, 179.78	4.024, 179.78	4.024, 179.78
		± 0.052, 0.30	± 0.053, 0.21	± 0.017

Table 1: Comparative results for ellipse-fitting techniques implemented in EllipseFit. Eigenvector = Shape matrix eigenvectors (Shimamoto and Ikeda, 1976). Radial = Mean radial length (Mulchrone, et al, 2003; Mulchrone, 2005). Hyperboloidal = Hyperboloidal vector mean (Yamaji, 2008). From Vollmer (2010).

Shape-matrix eigenvector (Shimamoto and Ikeda, 1976), mean radial length (Mulchrone et al., 2003), and hyberbolic vector mean (Yamaji, 2008) ellipse-fitting methods give precisely identical results.

7.1   Shape Matrix Eigenvectors

[Documentation in preparation]

7.2   Mean Radial Length (MRL)

[Documentation in preparation]

7.3   Hyperbolic Vector Mean

[Documentation in preparation]

7.4   Bootstrap Error Analysis

[Documentation in preparation]
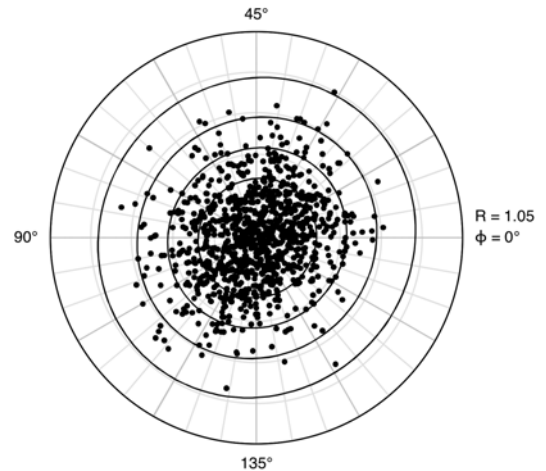
Figure 38: The best-fit strain ellipse is simply the hyperboloidal vector mean, which gives identical values to other methods (Yamaji 2008; Vollmer, 2010). Error analysis is shown by an equidistant azimuthal graph of bootstrap results of 1000 resamples from oolite data. The mean vector of the bootstrap mean vectors is rotated to C. The dispersion of the points is a measure of the error in the best-fit ellipse.

7.5   Simple Means and Centroids

[Documentation in preparation]

8.   Ellipsoid Calculation

For regional strain studies it is generally necessary to determine the three-dimensional strain ellipsoid, with three stretches and their orientations, normally expressed as trends and plunges. This can be simplified if assumptions can be made about the relationship between foliations and strain, for example slaty cleavage is commonly assumed perpendicular to the minimum stretch. However, in the general case it is necessary to determine the two-dimensional strain on a number of different planes through a sample (or outcrop where it can be considered homogeneous), and combine them to determine the strain ellipsoid in three dimensions. This is a difficult mathematical problem, and numerous solutions have been proposed (e.g., Shimamoto and Ikeda 1976; Owens, 1984; Robin, 2002; Shan, 2008; Mookerjee and Nickleach, 2011). EllipseFit implements the method of Shan (2008) as discussed in Section 8.2.

8.1 Global Coordinates and Sample Collection

The two-dimensional strain ellipses considered thus far have been referred to X, Y coordinates, where X is to the right, and Y is down the image. These coordinate axes are indicated by the blue lines on the top and left of the *Image Window*. The angle ϕ is the positive angle (clockwise) from X. This coordinate system was chosen to simplify the relationship to the *global coordinates* referred to here as X', Y', Z', and to simplify the calculation of the three-dimensional strain ellipsoid. The global coordinates are equivalent to North, East, Down (NED).

In Figure 39 the gray plane is a *section plane* that corresponds to an image analyzed for two-dimensional strain as discussed in earlier chapters. The X axis is parallel to the strike of the plane, using the standard *right hand rule* (e.g., Pollard and Fletcher, 2005), as shown in Figure 37. The strike is given by θ, the clockwise angle from North, the standard azimuth in degrees. The dip of the plane is the angle δ. The calculated strain ellipse is given by R = A/B = L_{Max}/L_{Min}, and ϕ, the angle from X, which is its *pitch* in global coordinates. This is referred to here as a *section ellipse*.

In order to calculate the strain ellipsoid from the section ellipses, each section ellipse must undergo a coordinate transformation from local X, Y coordinates to global X', Y', Z' coordinates. This is done automatically by EllipseFit, but the user must take great care to properly prepare samples. Time taken at this stage will save much aggravation later on.

A sample collected in the field must be carefully oriented, recording its strike and dip (other conventions are fine, but the strike is the X coordinate axis so is used here). A suitable marking is a *strike arrow* and a *dip tick* (Figure 39), if possible on a surface that is not
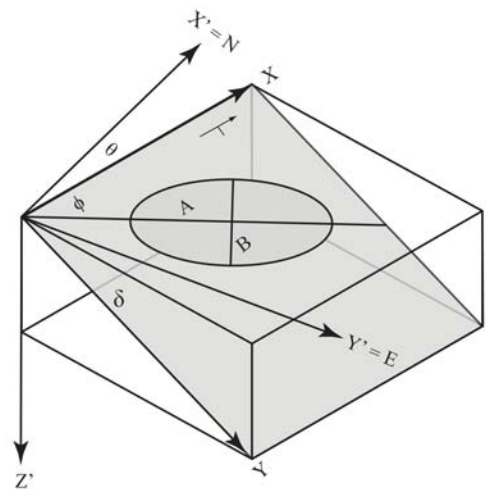

Figure 39: Coordinate system for section ellipses. The global coordinates are X' = North, Y' = East, and Z' = Down (NED). The plane with the section ellipse has a strike, θ (using the right hand rule), and dip, δ. The section ellipse has a pitch, ϕ, and R = A/B, where A and B are the maximum and minimum axes. A suggested strike arrow and dip tick marking is shown.

overhanging.

A minimum of three sections must be made through the sample, although more is preferred. Shan's method (Section 8.2) relaxes this requirement if lineation data is used as well, but Vollmer (2010) showed that the error range in natural samples can be large, so a minimum of three sections is recommended. If available, lineation data can supplement the section ellipses (Section 8.2).

The sections should be made at high angles to each other, but it does not need to be 90°, a restriction of some methods (e.g., Shimamoto and Ikeda, 1976). In making the sections be careful not to destroy the strike arrow and dip tick (it happens). The sample can then be taken outside, away from magnetic fields, and reoriented. The strikes and dips of the section planes can then be measured, and a strike arrow and dip tick marked on each face. The faces can then be photographed, or thin sections made, and photographed. Keeping thin sections correctly oriented is challenging, keep the strike arrow parallel to one side and pointing right.

To minimize confusion, make sure each photograph is oriented with the *section strike to the right*, and with the *dip line down*. Careful photography is best, but EllipseFit can rotate an image an arbitrary amount if necessary (see Chapter 12 Image Analysis). It is better to do it now than after digitizing the data, although EllipseFit can rotate the data if needed (see Chapter 11 Data Transformation).

One last *important* detail is to keep track of the viewing direction. The *strike arrow must point to the right* in the section image. This means it is dipping towards you. If the strike arrow points left, you are looking at the *underside* of the section and it is dipping away from you. If so, you need to *flip the image horizontally* about a vertical axis. EllipseFit can do this (Edit > Rotate Image > Flip Horizontal), and it is better to fix the image before digitizing. Vertical sections are not a problem if the recorded strike is kept to the right in the images.

If one is lucky to have outcrops with well exposed sections the process is greatly simplified, but the same principles apply.

Fields	Alternate	Symbol	Definition
N			Datum number
X', Y', Z'			Global coordinates (North, East, Down)
X, Y			Local coordinates, normally strike and dip line
Strike	Theta	θ	Strike of section following right-hand rule
Dip	Delta	δ	Dip of section plane from horizontal
Max, Int, Min	A, B, C		Axes of an ellipsoid
Max, Min	A, B		Axes of a sectional ellipse
R			Strain ratio, Max/Min
Phi	Pitch	ϕ	Angle in XY from X to ellipse axis Max
R*			Best-fit estimate of R
Phi*		ϕ^*	Best-fit estimate of ϕ
Delta R		ΔR	Misfit between R* and R
Delta Phi		$\Delta\phi$	Misfit between ϕ^* and ϕ
S1, S2, S3		S1, S2, S3	Principal stretches
Trend		t1, t2, t3	Trend of ellipsoid axis
Plunge		p1, p2, p3	Plunge of ellipsoid axis

Table 2: Data file field headers and corresponding symbols. The headers define columns in data files read and written by EllipseFit. .

8.2 Shan Ellipsoid Calculation

Shan's method for determining the strain ellipsoid from section ellipses has similarities to the methods of Owens (1984) and Robin (2002), as they are all direct non-iterative calculations. Shan's method, however, also allows the inclusion of stretching lineation data, so has additional flexibility. Ellipsoids can be represented by *shape matrixes,* and the solution desired is the optimal shape matrix. Each section ellipse, or section lineation, adds one or two linear equations describing the shape matrix, which can be solved as an eigenvalue problem. Shan solved the problem by assuming the matrix can be located on a six-dimensional hypersphere centered at the origin, and recognized that the smallest eigenvector of the data matrix is an optimal solution. EllipseFit is the first available implementation of Shan's method.

Before giving an example calculation, it is useful to compare it with some other methods. Shan's method has been tested on synthetic and natural samples, the following are some of the results of Vollmer (2010). Owens (1984) tested his method on a sample of slate from Dinorwic North Wales, for which the strains had been calculated from reduction spots on 8 sections. His data was also used by Launeau and Robin (2005) to test Robin's (2002) method. Table 3 shows results of Vollmer's (2010) tests on Shan's method using Owen's data.

j	θ	δ	A	B	R	φ	R*	φ*	ΔR	Δφ	RT*	φT*	ΔRT	ΔφT
1	302	78	16.5	4.5	3.670	165	3.083	165.700	0.587	0.700	3.082	165.700	0.002	0.000
2	301	77	9.5	3.5	2.710	166	3.076	165.380	0.366	0.620	3.075	165.380	0.005	0.000
3	302	75	20.5	6.8	3.010	166	3.024	165.310	0.014	0.690	3.023	165.310	0.003	0.010
4	201	71	37.0	6.0	6.170	173	6.418	172.780	0.248	0.220	6.420	172.780	0.001	0.000
5	178	71	7.5	1.5	5.000	0	4.618	179.090	0.382	0.910	4.618	179.090	0.002	0.000
6	18	79	16.7	3.0	5.570	10	5.923	7.870	0.353	2.130	5.924	7.870	0.004	0.000
7	17	78	22.0	4.0	5.500	8	5.792	7.710	0.292	0.290	5.793	7.710	0.003	0.000
8	19	78	18.0	3.0	6.000	7	5.987	8.200	0.013	1.200	5.989	8.200	0.001	0.000

Table 3: Results of test of Shan's (2008) method using data from Owens (1984). R*, φ* are the calculated b* (Table 4) section ellipses. Misfits ΔR, Δφ indicate the error between calculated and measured ellipses. Calculated section ellipses were used to back-calculate bT* (Table 4) and RT*, φT*. Misfits ΔRT, ΔφT indicate that the method does retrieve b*. From Vollmer (2010).

The test involves calculating the strain ellipsoid from the section ellipses, then from the calculated ellipsoid, determining the two-dimensional sections corresponding to the input data. These are reported as R*, φ* in the table. The difference is a *residual.* These are reported as ΔR, Δφ in the table. An additional result is shown by using the calculated section ellipses to calculate an ellipsoid. These are reported as ΔRT, ΔφT, and are negligible indicating success in retrieving the ellipsoid.

Table 4 shows the results of the ellipsoid calculation from this sample as calculated using the methods of Owens (1984), Robin (2002), and Shan (2008). The results are compared graphically in Figure 40. The calculations and graphs were done in EllipseFit 2 (Vollmer, 2011) and Orient 2 (Vollmer, 2012). There negligible differences between the results using the methods of Robin and Shan, the results using the method of Owen deviate a small amount from them.

Axis	Owens	Robin	Shan (b*)	b**
S1	2.340	2.626	2.565	2.567
t1	29.000	37.100	34.960	34.970
p1	10.000	11.300	10.890	10.890
S2	1.197	1.112	1.131	1.131
t2	122.000	129.500	127.350	127.360
p2	14.000	11.700	12.230	12.230
S3	0.357	0.343	0.345	0.345
t3	265.000	264.500	264.440	264.440
p3	73.000	73.600	73.510	73.510

Table 4. Comparison of calculated strain ellipsoids. Owens from Owens (1984). Robin from Launeau and Robin (2005), unweighted method of Robin (2002). Shan (b*) from Vollmer (2010), Shan's (2008) method. b** is a test to retrieve b*. The data is graphed in Figure 38. From Vollmer (2010).
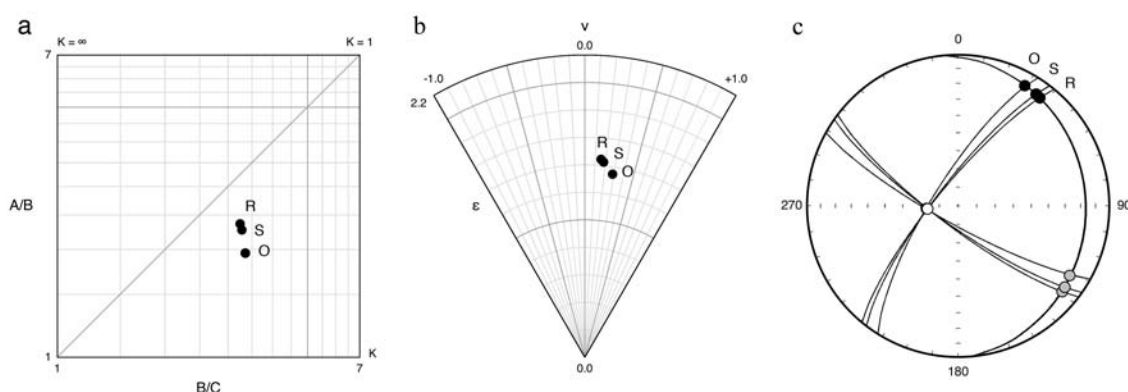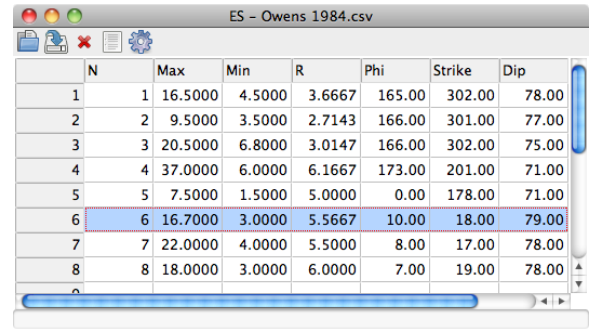

Figure 40. Comparison of calculated strain ellipsoids. O = Owens (1984). R = Launeau and Robin (2005) using unweighted method of Robin (2002). S = EllipseFit using Shan's (2008) method. From Vollmer (2010).

The file:

ES - Owens 1984.csv

contains the 8 section ellipse data from Owens (1984). Open this file in EllipseFit. The data as displayed in the Data Window is shown in Figure 41. There are 8 section ellipses, for each there is the Max, and Min (the axial lengths L_{Max}, L_{Min}), the strain ratio R = Max / Min, Phi (ϕ), the pitch of R from the X axis (X = strike), the strike angle (θ), and the dip angle (δ) (see Figure 39). This is data then, that, in EllipseFit, would be determined from oriented photographs of each of the 8 sections.

Select the command *Analyze > Calculate Ellipsoid* and the Calculate Ellipsoid Dialog is displayed as in Figure 42. The results will be written to the *Log Window*. Checking *Append results* will append the ellipsoid results to the open *Data Window*, so it can be plotted on Hsu and Nadia graphs. Check *Save orientations* to save the trends and plunges of the principal axes to a file that can be opened in Orient 2 (Vollmer, 2010) for plotting the axes on spherical projections.

Figure 41: The section data from a sample of slate from Dinorwic, North Wales from Owens (1984), displayed in the EllipseFit *Data Window*.

The *Bootstrap* option performs a bootstrap-type error analysis, using the number of resamples specified in the *Resamples* edit box, 5000 is the default value. Finally, the *Save bootstrap* will save the 5000 results of the resampling, which is normally unnecessary. Press *OK* to start the calculation. You will be prompted to save the orientation data files, and shortly the results appear in the Data Window (Figure 43) and the *Log Window*.
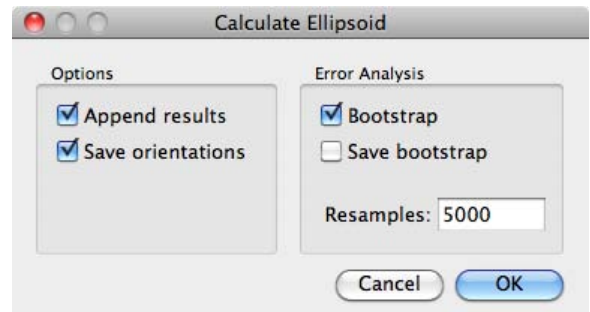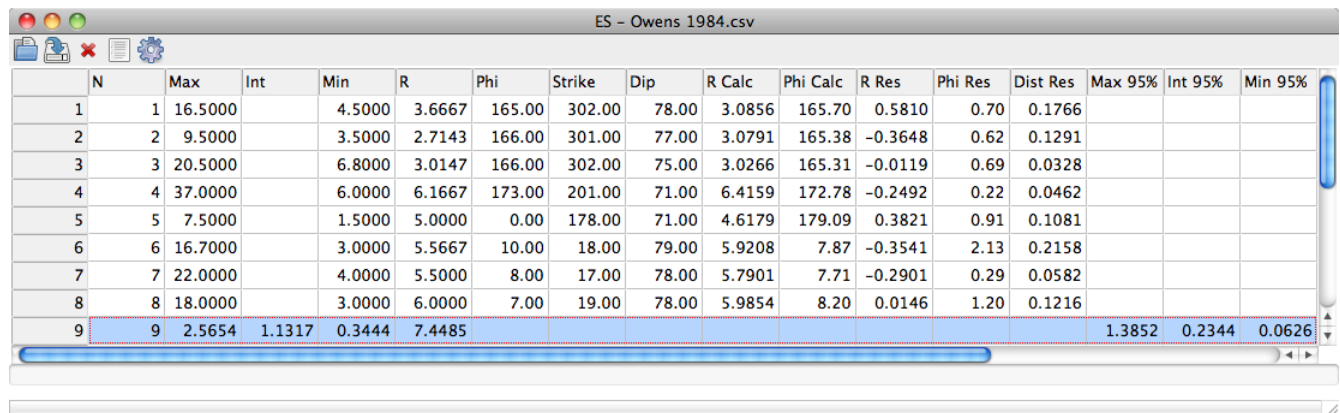

Figure 42: EllipseFit's *Calculate Ellipsoid Dialog*.

The Data Window now displays the ellipsoid principal axes Max, Int, Min as stretches (S_{Max}, S_{Int}, S_{Min}), and 95% confidence intervals calculated by the bootstrap. The section ellipses show the back-calculated values for R and ϕ, and the corresponding residuals. The last columns the *distance residuals*, which are the hyperbolic distance residuals.

	N	Max	Int	Min	R	Phi	Strike	Dip	R Calc	Phi Calc	R Res	Phi Res	Dist Res	Max 95%	Int 95%	Min 95%
1	1	16.5000		4.5000	3.6667	165.00	302.00	78.00	3.0856	165.70	0.5810	0.70	0.1766			
2	2	9.5000		3.5000	2.7143	166.00	301.00	77.00	3.0791	165.38	-0.3648	0.62	0.1291			
3	3	20.5000		6.8000	3.0147	166.00	302.00	75.00	3.0266	165.31	-0.0119	0.69	0.0328			
4	4	37.0000		6.0000	6.1667	173.00	201.00	71.00	6.4159	172.78	-0.2492	0.22	0.0462			
5	5	7.5000		1.5000	5.0000	0.00	178.00	71.00	4.6179	179.09	0.3821	0.91	0.1081			
6	6	16.7000		3.0000	5.5667	10.00	18.00	79.00	5.9208	7.87	-0.3541	2.13	0.2158			
7	7	22.0000		4.0000	5.5000	8.00	17.00	78.00	5.7901	7.71	-0.2901	0.29	0.0582			
8	8	18.0000		3.0000	6.0000	7.00	19.00	78.00	5.9854	8.20	0.0146	1.20	0.1216			
9	9	2.5654	1.1317	0.3444	7.4485									1.3852	0.2344	0.0626

Figure 43: The *Data Window* after calculating the optimal ellipse using Shan's method.

The Log Window reports the following:

```
Best-Fit Ellipsoid Calculations
ES - Owens 1984
2014-06-02 19:51:39
==============================
N = 8
Ellipsoid axes as stretches:
Maximum (A)      = 2.565
Trend            = 35.02
Plunge           = 10.90
Intermediate (B) = 1.132
Trend            = 127.41
Plunge           = 12.22
Minimum (C)      = 0.344
Trend            = 264.44
Plunge           = 73.51
Root mean square of section residuals:
R +/-            = 0.333
Phi +/-          = 0.85
Distance +/-     = 0.126
See data grid for section residuals
Bootstrap confidence intervals (5000 resamples)
Maximum (A):
  Stretch +/-    = 0.973
  Stretch 95%    = 1.385
  Stretch 99%    = 3.603
  Trend +/-      = 0.186
  Trend 95%      = 0.269
  Trend 99%      = 0.369
  Plunge +/-     = 0.037
  Plunge 95%     = 0.058
  Plunge 99%     = 0.083
Intermediate (B):
  Stretch +/-    = 0.106
  Stretch 95%    = 0.234
  Stretch 99%    = 0.415
  Trend +/-      = 0.187
  Trend 95%      = 0.273
  Trend 99%      = 0.382
  Plunge +/-     = 0.041
  Plunge 95%     = 0.057
  Plunge 99%     = 0.073
Minimum (C):
  Stretch +/-    = 0.030
  Stretch 95%    = 0.063
```

```
Stretch 99%    = 0.117
Trend +/-      = 0.031
Trend 95%      = 0.043
Trend 99%      = 0.056
Plunge +/-     = 0.014
Plunge 95%     = 0.020
Plunge 99%     = 0.026
```

This includes all 3 principal stretches, and their trends and plunges, with measures of error. To view the results graphically, first select *Analyze > Flinn Graph.* A Flinn graph (Section 9.1) is a graph of the ratios A/B = S_{Max}/S_{Int} versus B/C = S_{Int}/S_{Min}. , and is commonly used for displaying strain ellipsoid data (e.g. Ramsay and Huber).
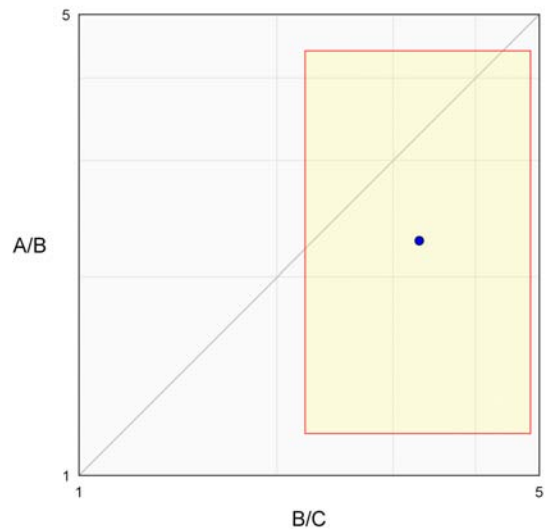

Figure 44: Flinn graph of the ellipsoid axial ratios determined from the Shan calculation, with a 95% confidence region.

Now select *Analyse > Nadia Graph*, to display the results on a Nadai graph. A Nadai graph (Nadia, 1950; Hossack, 1968; Section 9.2) is based on *natural*, or logarithmic strain, which is also the basis for the hyberboldal projections discussed in Section 6.3. This provides an undistorted representation of the deviatoric strains and is preferred by many for that reason (Brandon, 1995).
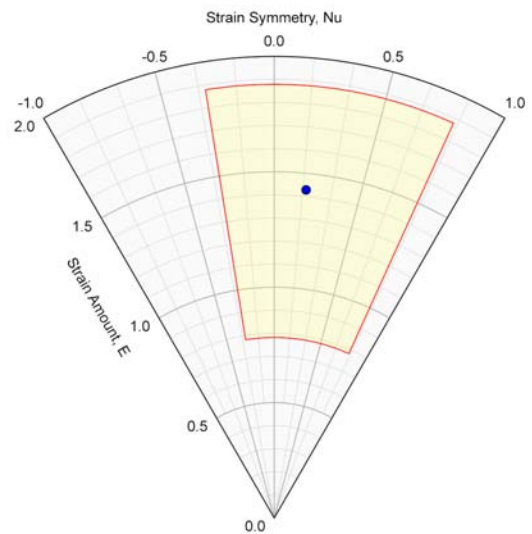

Figure 45: Nadai graph of the ellipsoid axial ratios determined from the Shan calculation with a 95% confidence region.

The calculated strain has large 95% error region as shown in both graphs. Examining the data (Figure 43), shows that section 6 has the largest distance residual. Select it, delete it and preform the ellipsoid calculation again. Figure 46 shows the updated Flinn graph, which now shows both solutions.
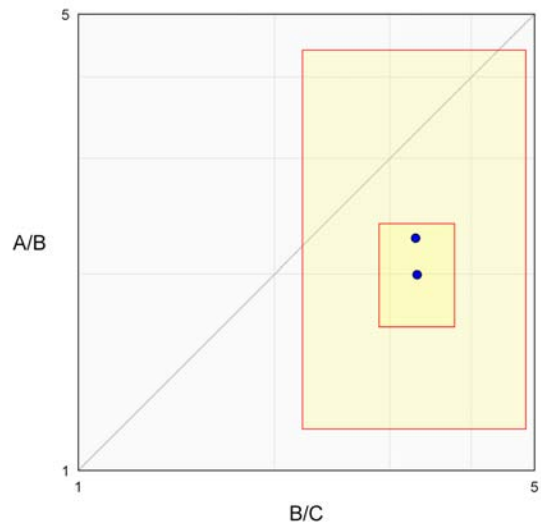

Figure 46: Flinn graph of the ellipsoid axial ratios determined from the Shan calculation, with 95% confidence regions, after deleting section 6.

Similarly the Nadia graph has been updated to reflect the newly calculated results.
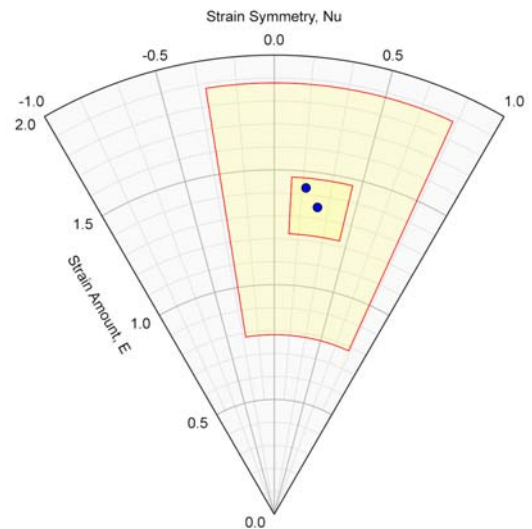

Figure 47: Nadia graph of the ellipsoid axial ratios determined from the Shan calculation, with 95% confidence regions, after deleting section 6.

Finally, the resulting axes are plotted on a lower hemisphere equal-area projection using Orient 2.1.2 (Vollmer, 2010). The strain axes calculated from all 8 sections are plotted as circles, and the axes section 6 removed are plotted as diamonds. Red = S_{Max}, green = R_{Int}, blue = R_{Min}.
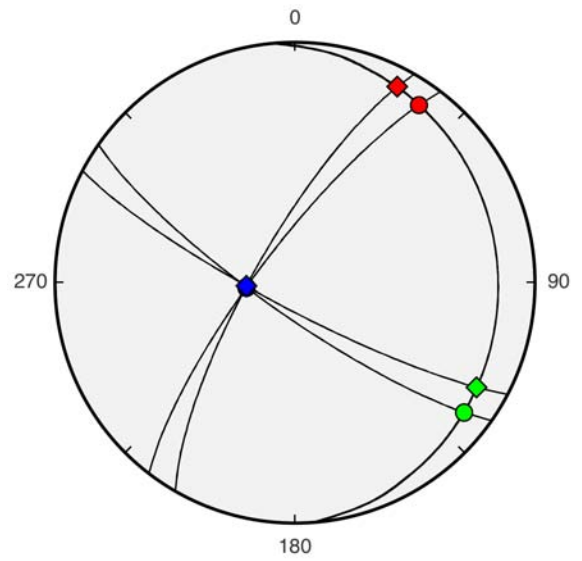

Figure 48: Lower hemisphere equal-area projection of the strain ellipsoid axes. Circles are the axes calculated from all 8 sections, diamonds with section 6 removed. Red = S_{Max}, green = R_{Int}, blue = R_{Min}.

[Documentation in preparation]

Axis	bT14*	bT24*	bT34*	bT45*	bT46*	bT47*	bT48*	bT56*	bT57*	bT58*
S1	2.569	2.570	2.570	2.570	2.569	2.569	2.570	2.568	2.568	2.570
t1	35.060	35.100	35.010	35.180	35.030	35.030	35.010	35.230	35.220	35.010
p1	10.900	10.910	10.890	10.930	10.900	10.900	10.890	10.940	10.940	10.890
S2	1.130	1.131	1.130	1.132	1.130	1.130	1.130	1.133	1.133	1.130
t2	127.450	127.490	127.400	127.570	127.420	127.420	127.400	127.620	127.610	127.400
p2	12.210	12.200	12.220	12.190	12.220	12.220	12.220	12.180	12.180	12.220
S3	0.344	0.344	0.344	0.344	0.344	0.344	0.344	0.344	0.344	0.344
t3	264.450	264.440	264.450	264.440	264.450	264.450	264.450	264.440	264.440	264.450
p3	73.510	73.520	73.510	73.520	73.510	73.510	73.510	73.520	73.520	73.510

Table 5: Results of test of ellipsoid-fitting using two ellipses and six lineations from synthetic section ellipses calculated from b* (Table 4). For ten tests six of the eight RTj values were omitted. Subscripts indicate the sections with RTj data. Results are all identical down to round-off error.

Axis	b14*	b24*	b34*	b45*	b46*	b47*	b48*	b56*	b57*	b58*
S1	nan	3.422	4.379	3.196	3.389	3.371	3.469	3.126	3.301	3.127
t1	nan	41.760	47.150	43.140	20.310	20.330	20.320	42.680	45.960	37.500
p1	nan	11.690	12.580	12.310	8.060	8.060	8.060	12.240	12.790	11.280
S2	nan	0.902	0.836	1.052	0.584	0.585	0.578	0.301	1.054	1.021
t2	nan	133.950	139.230	135.430	235.100	234.930	235.570	264.470	138.190	129.850
p2	nan	10.430	9.240	10.370	80.220	80.240	80.160	73.780	9.730	11.610
S3	nan	0.323	0.273	0.297	0.505	0.507	0.499	0.561	0.287	0.313
t3	nan	264.630	264.590	264.450	111.090	111.110	111.110	264.470	264.450	264.490
p3	nan	74.230	74.300	73.800	5.510	5.470	5.600	73.780	73.830	73.700

Table 6: Test of ellipsoid-fitting using two ellipses and six lineations from eight measured section ellipses (Table 5). For ten tests six of the eight Rj values were omitted. Subscripts indicate the sections with Rj data. Results are highly variable, especially as axial ratios, which are plotted in Fig. 8.
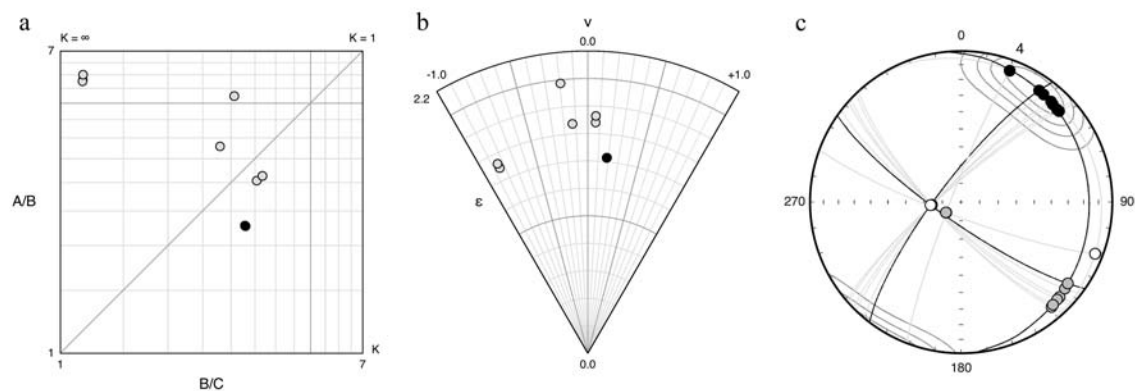
Figure 49. Test of ellipsoid-fitting using two ellipses and six lineations from eight measured section ellipses (Table 5). For ten tests six of the eight Rj values were omitted. Subscripts indicate the sections with Rj data. Results are highly variable, especially as axial ratios.

9. Ellipsoid Data Graphs

[Documentation in preparation]

9.1 Flinn Graphs

[Documentation in preparation]

A Flinn graph is a graph of the ratios A/B = S_{Max}/S_{Int} versus B/C = S_{Int}/S_{Min}, and is commonly used for displaying strain ellipsoid data (e.g. Ramsay and Huber).

As with the ellipse graphs, the Flinn and Nadia graphs are interactive, selecting a point in one will automatically select the corresponding data point on the other graph, and in the *Data Window*.
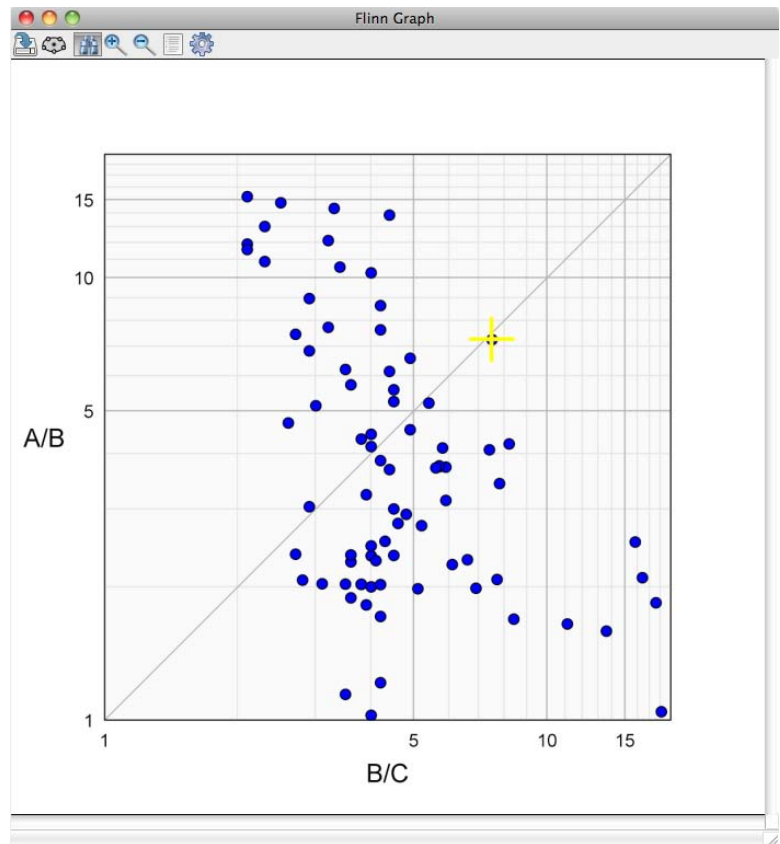

Figure 50: Log Flinn graph displaying deformed pebble ellipsoids, Bygdin area, Norway, from Hossack, 1968. This graph is interactive, with the *Binoculars Icon* selected, data points can be selected and will be simultaneously updated on the Nadai graph and in the *Data Window*, the selected data point is also displayed in Figure 51.

9.2   Nadai Graphs

[Documentation in preparation]

The Nadai graph (Nadia, 1950; Hossack, 1968; Section 9.2) is based on *natural*, or logarithmic strain, which is also the basis for the hyberboldal projections discussed in Section 6.3. This provides an undistorted representation of the deviatoric strains and is preferred by many for that reason (Brandon, 1995).
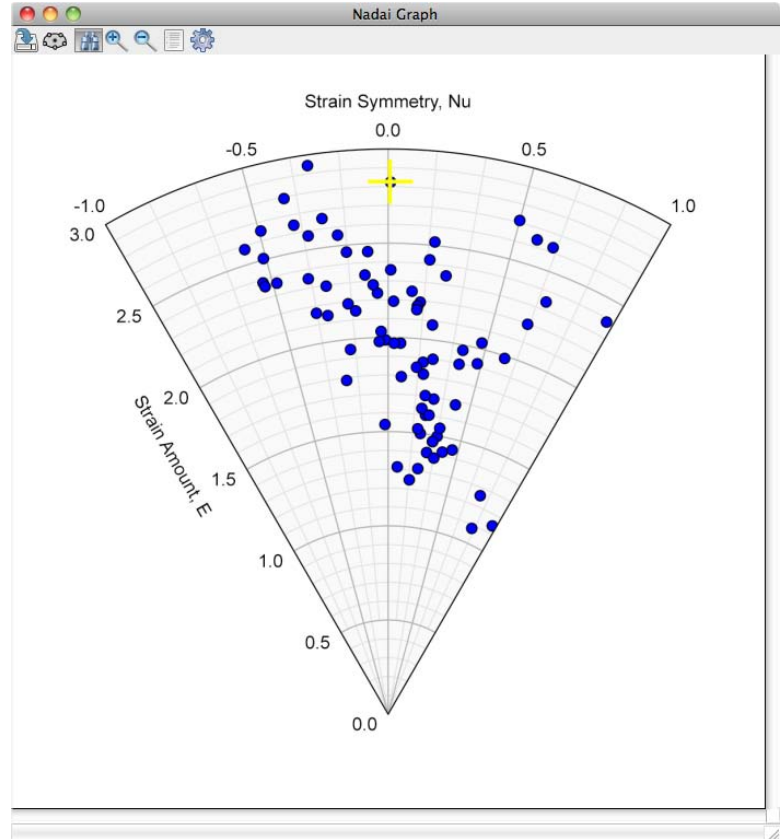

Figure 51. Nadia graph displaying deformed pebble ellipsoids, Bygdin area, Norway, from Hossack, 1968. This graph is interactive, with the *Binoculars Icon* selected, data points can be selected and will be simultaneously updated on the Flinn graph and in the *Data Window*, the selected data point is also displayed in Figure 48.
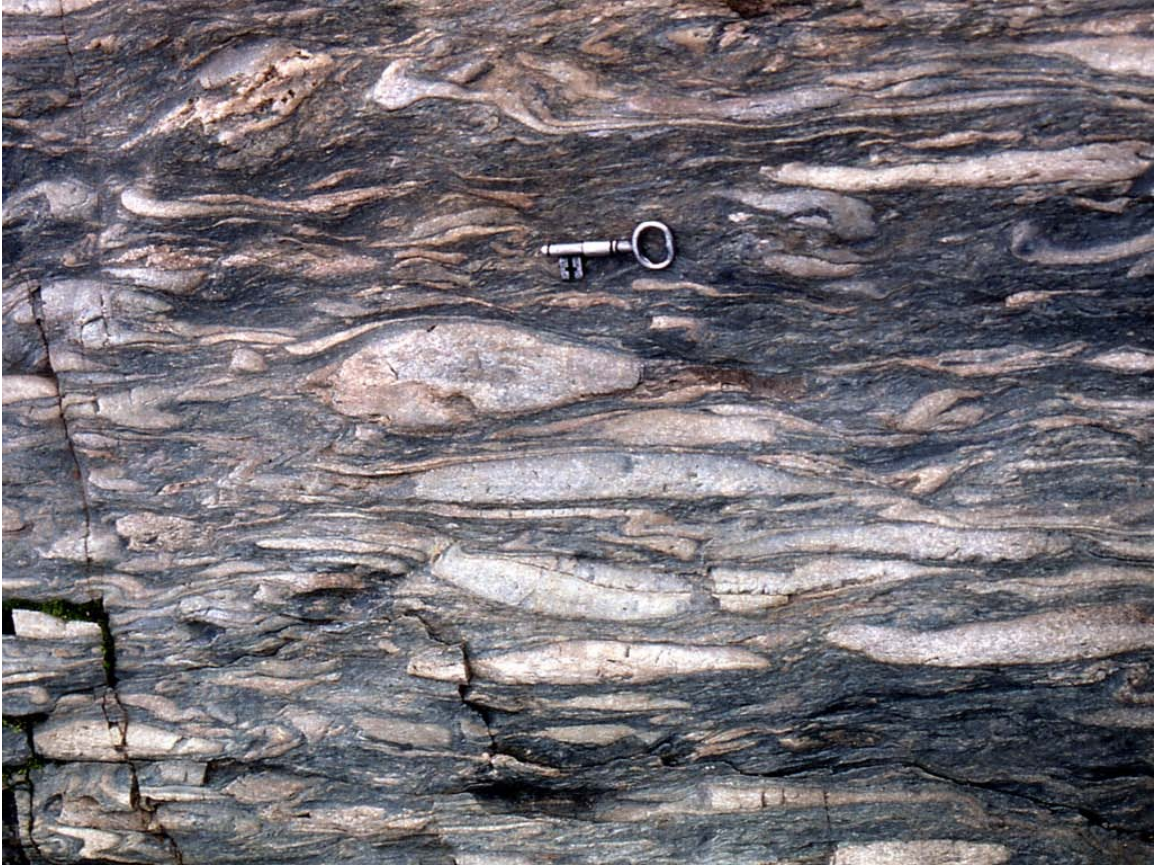
Figure 52. Deformed pebble conglomerate, Bygdin area, Norway, where the data graphed in Figures 50 and 51 was collected by Hossack (1968). Photograph by F. W. Vollmer.

Acknowledgements

References

Brandon, M.T, 1995. Analysis of geological strain data in strain-magnitude space. Journal of Structural Geology, 17, 1375-1385.

Cloos, E., 1947. Oolite deformation in the South Mountain Fold, Maryland. Geological Society of America Bulletin, 58, 843-918.

Cloos, E., 1971. Microtectonics Along the Western Edge of the Blue Ridge, Maryland and Virginia. The Johns Hopkins Press, Baltimore and London, 234 p.

Crespi, J.M., 1986. Some guidelines for the practical application of Fry's method of strain analysis. Journal of Structural Geology 16, p. 1327-1330.

Davis, J.C., 1986. Statistics and Data Analysis in Geology. Wiley, 646 p.

Dirringer, S., and Vollmer, F.W., 2013. A test of the analytical Wellman and mean polygon moment ellipse methods of strain analysis using a sample of deformed Ordovician graptoliferous slate from the Taconic orogen, New York. Geological Society of America Abstracts with Programs, 247-52.

Dunne, W.M., Onasch, C.M., Williams, R.T., 1990. The problem of strain-marker centers and the Fry method. Journal of Structural Geology 12, p. 933-1990.

Dunnet, D., 1969. A technique of finite strain analysis using elliptical particle. Tectonophysics 7, 117-136.

Dunnet, D., and Siddans, A.W.B., 1971. Non-random sedimentary fabrics and their modification by strain. Tectonophysics, 12, 307-325.

Efron, B., 1979. Bootstrap methods: Another look at the jackknife. Annals of Statistics 7, 1-26.

Elliott, D., 1970. Determination of finite strain and initial shape from deformed elliptical objects. Geological Society of America Bulletin 81, 2221-2236.

Erslev, E.A., 1988. Normalized center-to-center strain analysis of packed aggregates. Journal of Structural Geology 10, 201-209.

Erslev, E.A., Ge, H., 1990. Least squares center-to-center and mean object ellipse fabric analysis. Journal of Structural Geology 8, 1047-1059.

Fisher, N.I., Lewis, T., and Embleton, B.J.J., 1987. Statistical Analysis of Spherical Data. Cambridge University Press, 329 p.

Flinn, D., 1962. On folding during three-dimensional progressive deformation. Quarterly Journal of the Geological Society of London, 118, p. 385-433.

Flinn, D., 1978. Construction and computation of three-dimensional deformations. Journal of the Geological Society of London, 135, p. 291-305.

Fossen, H, 2010. Structural geology. Cambridge University Press, 463 p.

Fry, N., 1979. Random point distributions and strain measurement in rocks. Tectonophysics 60, 806-807.

Hanna, S.S., Fry, N., 1979. A comparison of methods of strain determination in rocks from southwest Dyfed (Pembrokeshire) and adjacent areas. Journal of Structural Geology 2, 155-162.

Hobbs, B.E., Means, W.D., and Williams, P.F., 1976. An outline of structural geology. Wiley, New York, 571 pp.

Hossack, J.R., 1968. Pebble deformation and thrusting in the Bygdin area (Southern Norway). Tectonophysics 5, 315-339.

Jensen, 1981. On the hyperboloid distribution. Scandinavian Journal of Statistics 8, 193-206.

Launeau, L., and Pierre-Yves F. Robin. P.F., 2005. Determination of fabric and strain ellipsoids from measured sectional ellipses—implementation and applications. Journal of Structural Geology 27, 2223-2233.

Lisle, R.J., 1985. Geological Strain Analysis, A Manual for the Rf/φ Technique. Pergamon Press, Oxford.

Mardia, K.V., 1972. Statistics of Directional Data. Academic Press, 329 p.

Marshak, S., and Mitra, G., 1988. Basic methods of structural geology. Prentice Hall, 446 p.

McNaught, M.A., 1994. Modifying the normalized Fry method for aggregates of non-elliptical grains. Journal of Structural Geology 16, 493-503.

McNaught, M.A., 2002. Estimating uncertainty in normalized Fry plots using a bootstrap approach. Journal of Structural Geology, 24, p. 311-322.

Mitra, S., 1978. Microscopic deformation mechanisms and flow laws in quartzites within the South Mountain anticline. Journal of Geology 86, p. 129-152.

Mookerjee, M., and Nickleach, S., 2011. Three-dimensional strain analysis using Mathematica. Journal of Structural Geology 33, p. 1467-1476.

Mulchrone, K.F., O'Sullivan, F., Meere, P.A., 2003. Finite strain estimation using the mean radial length of elliptical objects with bootstrap confidence intervals. Journal of Structural Geology 25, 529-539.

Mulchrone, K.F. 2005. An analytical error for the mean radial length method strain analysis. Journal of Structural Geology 27, 1658-1665.

Mulchrone, K.F., 2013. Fitting the void: Data boundaries, point distributions and strain analysis. Journal of Structural Geology 46, 22-33.

Nadai, A., 1950. Theory of Flow and Fracture of Solids. McGraw-Hill, New York, 572 p.

Onasch, C.M., 1986. Ability of the Fry method to characterize pressure- solution deformation. Tectonophysics 122, 187-193.

Owens, W.H., 1984. The calculation of a best-fit ellipsoid from elliptical sections on arbitrarily orientated planes. Journal of Structural Geology 6, 571-578.

Pollard, D.D. and Fletcher, R.C., 2005. Fundamentals of structural geology. Cambridge University Press, Cambridge, 463 500 p.

Ragan, D.M., 1985. Structural Geology, An Introduction to Geometrical Techniques, 3rd Ed. John Wiley and Sons, Inc. 393 p.

Ragan, D.M., and Groshong, R.H., 1993. Strain from two angulars of shear. Journal of Structural Geology, v. 15, p. 1359-1360.

Ragan, D.M., 2009. Structural Geology, An Introduction to Geometrical Techniques, 4th Ed. John Wiley and Sons, Inc. 393 p.

Ramsay, J.G. and Huber, M. I., 1983. The Techniques of Modern Structural Geology: Volume 1: Strain. Analysis, Academic Press, London, 307 p.

Ramsay, J.G., 1967. Folding and Fracturing of Rocks. McGraw-Hill, 568 p.

Robin, P.F., 2002. Determination of fabric and strain ellipsoids from measured sectional ellipses – theory. Journal of Structural Geology 24, 531-544.

Rogers, D.F. And Adams, J.A., 1976. Mathematical Elements for Computer Graphics. McGraw-Hill, New York, 239 p.

Shan, Y., 2008. An analytical approach for determining strain ellipsoids from measurements on planar surfaces. Journal of Structural Geology 30, 539-546.

Shan, Y., and Xiao, W., 2011. A statistical examination of the Fry method of strain analysis. Journal of Structural Geology, v. 33, p. 1000-1009.

Shimamoto, T., Ikeda, Y., 1976. A simple algebraic method for strain estimation from ellipsoidal objects: Tectonophysics 36, 315-337.

Steger, C., 1996. On the Calculation of Arbitrary Moments of Polygons, Technical Report FGBV-96-05, Forschungsgruppe Bildverstehen (FG BV), Informatik IX Technische Universitat Munchen, Germany, 18 p.

Twiss, R.J. and Moores, E., 2007. Structural geology, 2nd edition. W.H. Freeman, New York, 736 pp.

Van der Pluijm, B.A. and Marshak, S., 2004. Earth structure, 2nd edition. W.W. Norton, New York, 656 p.

Vollmer, F.W., 1995. C program for automatic for automatic contouring of spherical orientation data using a modified Kamb method: Computers & Geosciences 21, 31-49.

Vollmer, F.W., 2010. A comparison of ellipse-fitting techniques for two and three-dimensional strain analysis, and their implementation in an integrated computer program designed for field-based studies. Abstract T21B-2166, Fall Meeting, American Geophysical Union, San Francisco, California. [1]

Vollmer, F.W., 2011a. Automatic contouring of two-dimensional finite strain data on the unit hyperboloid and the use of hyperboloidal stereographic, equal-area and other projections for strain analysis. Geological Society of America Abstracts with Programs, v. 43, n. 5, p. 605. [2]

Vollmer, F.W., 2011b. Best-fit strain from multiple angles of shear and implementation in a computer program for geological strain analysis. Geological Society of America Abstracts with Programs, v. 43. [3]

Waldron, J.W.F., and Wallace, K.D., 2011. Objective fitting of ellipses in the centre-to-centre (Fry) method of strain analysis. Journal of Structural Geology 29, p.1430-1444.

Wellman, H.G., 1962, A graphic method for analyzing fossil distortion caused by tectonic deformation. Geological Magazine, 99, 384-352.

Wheeler, J., 1984. A new plot to display the strain of elliptical markers: Journal of Structural Geology 6, 417-423.

Hossack, J.R., 1968. Pebble deformation and thrusting in the Bygdin area (Southern Norway): Tectonophysics 5, 315-339.

Yamaji, A., 2008. Theories of strain analysis from shape fabrics: A perspective using hyperbolic geometry. Journal of Structural Geology 30, 1451-1465.

History

3.1.1
- Added the ability to open Microsoft Excel XLS (legacy) and XLSX formats, in addition to OpenDocument ODS spreadsheet, and delimited file (CSV, TSV) formats. In each case, a comment line starts with '//', and a header row identifying the data columns must precede the data rows.
- Fixed bug requiring "Max", "Min" data and header as well as "R" for ellipsoid calculation. Also now allows "Pitch" header in place of "Phi". Thanks to Kurt Burmeister for reporting this.
- Replaced timers with event messaging.
- Fixes to Analyze > Data Synthesis command, which failed in Windows. The collision tests counts have been increased to 10,000 x 10,000, which tightens adjacent particle contacts.

3.1.0
- Added bootstrap error analysis to ellipsoid calculations. This has some similarities to the kernel density estimation approach of Mookerjee and Nickleach (2011).
- Added saving of the ellipsoid axes orientations for plotting on spherical projections in Orient.
- Changed column headers A, B, C to Max, Int, Min to clarify the axial lengths. EllipseFit will open files with the old headers, but will save them using the new headers.
- Removed option to save files as "Space Delimited". This format potentially causes issues parsing files with spaces in the header column. EllipseFit will still open space delimited files with recognizable headers.
- Added 95% confidence regions to Nadai graph.
- Added 95% confidence regions to Flinn graph.
- Added option to save bootstrap ellipsoid axes.
- Added numerous options to Synthesize Data command. These include generating the strain ratio from a Gaussian normal distribution, generating particle size from a Gaussian normal distribution, generating a preferred orientation from a Von Mises circular distribution, generating centers at a truncated Poisson distribution. The latter is performed by randomizing the location in x, y and discarding collisions.
- Added an option to the Strain Map command to either plot scaled strain ellipses or particle axes.
- Implemented the maximum mean log likelihood function (MLLF) search procedure of Shan and Xiao (2011). This gives a high accuracy strain estimate from Fry-type data, that is, data from truncated Poisson distributions. It does not require ellipse data, and it is not subjective and is reproducible.
- Fixed auto-scaling on Fry graphs.
- Significant progress on the User Manual.

3.0.3 – 13 May 2014
- Added transforms to image to rotate, flip, strain, unstrain, etc. To strain or unstrain both image and data, transform the image first. This calculates the origin offset in the new bitmap. Then transform the data at (X0, Y0) = (0.0, 0.0) with "Rectify" checked.
- Added transform data to Wellman-type data.
- Changed default bootstrap resamples from 300 to 5000.
- Rewrote ellipse standard error and confidence interval methods. Changed from using resample trials to calculate standard error and Student T for confidence interval, to use resampled data for both. Non-bootstrap MRL uses analytical error and Student T following Mulchrone (2005).
- Added option to save bootstrap resample ellipses.

- Added option to plot 95% confidence regions on Polar and Rf/Phi graphs using analytical error.
- Fixed bug that was swapping A and B radii while digitizing polygons.

3.0.2 – 21 April 2014
- Fixed bug in fill ellipse routine causing hangs at high thresholds.
- Fixed bug causing crash when opening page size dialog.
- Added strain map.
- Added synthesize data to create data sets.
- Added transform data to strain, unstrain, shear, etc., data.
- Changed names of digitize routines to reflect the objects, e.g., center points, ellipses, polygons, instead of the results (e.g., polygon moment ellipse).
- Changed names of graphs to more common specific names attributing authors, Fry, Flinn, etc., instead of generic names.
- Internal change in form communication, from flags and timers to messages.
- Numerous additional fixes and changes.

3.0.1 – 6 April 2014
- Fixed bug effecting symbol colors in svg graphics.
- Cleaned up the polar graph.
- Fixed cursor status strings on graphs.
- Fixed up contouring preferences.
- Added axial ratio Flinn type graph.
- Added octahedral Nadai-Hsu type strain graph.
- Added ellipse digitizing with polygon fill and moments.
- Fixed file save warning.
- Numerous internal changes.

3.0.0 – 24 March 2014
- First public release.

3.0.0.28 - August 1, 2012
- Initial prerelease version.